Astroparticle Physics 80 (2016) 90–114

Contents lists available at ScienceDirect

Astroparticle Physics

journal homepage: www.elsevier.com/locate/astropartphys

Primordial Black Holes: Observational characteristics of the final evaporation

T.N. Ukwatta[a,*], D.R. Stump[b], J.T. Linnemann[b], J.H. MacGibbon[c], S.S. Marinelli[b], T. Yapici[b], K. Tollefson[b]

[a] Director's Postdoctoral Fellow, Space and Remote Sensing (ISR-2), Los Alamos National Laboratory, Los Alamos, NM 87545, USA
[b] Department of Physics and Astronomy, Michigan State University, East Lansing, MI 48824, USA
[c] Department of Physics, University of North Florida, Jacksonville, FL 32224, USA

ARTICLE INFO

Article history:
Received 12 October 2015
Revised 2 March 2016
Accepted 23 March 2016
Available online 29 March 2016

Keywords:
Primordial Black Holes
HAWC
Very high energy bursts
Gamma-ray bursts

ABSTRACT

Many early universe theories predict the creation of Primordial Black Holes (PBHs). PBHs could have masses ranging from the Planck mass to 10^5 solar masses or higher depending on the size of the universe at formation. A Black Hole (BH) has a Hawking temperature which is inversely proportional to its mass. Hence a sufficiently small BH will quasi-thermally radiate particles at an ever-increasing rate as emission lowers its mass and raises its temperature. The final moments of this evaporation phase should be explosive and its description is dependent on the particle physics model. In this work we investigate the final few seconds of BH evaporation, using the Standard Model and incorporating the most recent Large Hadron Collider (LHC) results, and provide a new parameterization for the instantaneous emission spectrum. We calculate for the first time energy-dependent PBH burst light curves in the GeV/TeV energy range. Moreover, we explore PBH burst search methods and potential observational PBH burst signatures. We have found a unique signature in the PBH burst light curves that may be detectable by GeV/TeV gamma-ray observatories such as the High Altitude Water Cerenkov (HAWC) observatory. The implications of beyond the Standard Model theories on the PBH burst observational characteristics are also discussed, including potential sensitivity of the instantaneous photon detection rate to a squark threshold in the 5–10 TeV range.

Published by Elsevier B.V.

1. Introduction

Many current theories of the early universe predict the production of primordial black holes (PBHs) [1]. Cosmological density fluctuations and other mechanisms such as those associated with phase transitions in the early universe could have created PBHs with masses of order of, or smaller than, the cosmological horizon size at the time of formation. Depending on the formation mechanism, PBHs could form at times from the Planck time[1] to 1 s after the Big Bang, or later. Hence the initial mass of a PBH could be as small as the Planck mass[2] or as massive as 10^5 solar mass, or higher.

In 1974, Hawking showed by convolving quantum field theory, thermodynamics and general relativity that a Black Hole[3] (BH) has a temperature inversely proportional to its mass and emits photon and particle radiation with thermal spectra [2]. As the BH emits this radiation, its mass decreases and hence its temperature and flux increase. A PBH that formed with an initial mass of $\sim 5.0 \times 10^{11}$ kg in the early universe should be expiring today [3] with a burst of high-energy particles, including gamma-rays in the MeV to TeV energy range. Thus PBHs are candidate gamma-ray burst (GRB) progenitors [4].

Confirmed detection of a PBH evaporation event would provide valuable insights into many areas of physics including the early universe, high energy particle physics and the convolution of gravitation with thermodynamics. Conversely, non-detection of PBH evaporation events in sky searches would place important limits on models of the early universe. One of the most important

* Corresponding author. Tel.: +1 5712342598; fax: +1 8666576210.
E-mail address: tilan.ukwatta@gmail.com (T.N. Ukwatta).

[1] Planck time $\left(\hbar G/c^5\right)^{1/2} \simeq 5.391 \times 10^{-44}$ s.

[2] Planck mass $(\hbar c/G)^{1/2} \simeq 2.176 \times 10^{-8}$ kg.

[3] Throughout this paper, we use the notation 'BH' when discussing a black hole irrespective of its formation mechanism or formation epoch and 'PBH' when referring to a black hole created in the early universe.

http://dx.doi.org/10.1016/j.astropartphys.2016.03.007
0927-6505/Published by Elsevier B.V.

Table 1
PBH burst limits on various distance scales: (1) from the 100 MeV extragalactic gamma-ray background assuming no PBH clustering [1,14], (2) from the Galactic 100 MeV anisotropy measurement [15], (3) from the Galactic antiproton flux [16] and (4) from Very High Energy direct burst searches [11].

Distance scale	Limit	Method
Cosmological scale	$< 10^{-6}$ pc^{-3}year^{-1}	(1)
Galactic scale	< 0.42 pc^{-3}year^{-1}	(2)
Kiloparsec scale	$< 1.2 \times 10^{-3}$ pc^{-3}year^{-1}	(3)
Parsec scale	$< 1.4 \times 10^{4}$ pc^{-3}year^{-1}	(4)

reasons to search for PBHs is to constrain the cosmological density fluctuation spectrum in the early universe on scales smaller than those constrained by the cosmic microwave background. There is particular interest in whether PBHs form from the quantum fluctuations associated with many different types of inflationary scenarios [1]. Detection or upper limits on the number density of PBHs can thus inform inflationary models.

PBHs may be detectable by virtue of several effects. For example, PBHs with planetary-scale masses may be detectable by their gravitational effects in micro-lensing observations [5]; or accretion of matter onto PBHs in relatively dense environments may produce distinct, observable radiation [6]. Such situations, however, should be rare and therefore difficult to use as probes of the cosmological or local PBH distribution. On the other hand, any PBHs with an initial mass of $\sim 5.0 \times 10^{11}$ kg is expected to explode today in a final burst of Hawking radiation. These events, out to a determinable distance, should be detectable at Earth as sudden bursts of gamma-rays in the sky. Numerous observatories have searched for PBH burst events using direct and indirect methods. These methods are sensitive to the PBH distribution at various distance scales. Observatories that observe photons or antiprotons at ~100 MeV can probe the cosmologically-averaged or Galactic-averaged PBH distribution whereas TeV observatories directly probe PBH bursts on parsec scales. Because it is possible that PBHs may be clustered at various scales, all these searches provide important information. We also note that the TeV direct search limits [7–13] apply not only to PBHs but to any nearby presently bursting black holes, regardless of their formation mechanism or formation epoch, and so equally constrain the number of local bursting BHs which may have formed in the more recent or current universe. Table 1 gives a summary of various search methods, the distance scales they probe and their current best limits.

The properties of the BH final burst depend on the physics governing the production and decay of high-energy particles. As the BH evaporates and loses mass over its lifetime, its temperature increases. The higher the number of fundamental particle degrees of freedom, the faster and more powerful will be the final burst from the BH. The details of the predicted spectra differ according to the high-energy particle physics model. In the Standard Evaporation Model (SEM) which incorporates the Standard Model of particle physics, a BH should directly Hawking-radiate the fundamental Standard Model particles whose de Broglie wavelengths are of the order of the black hole size [17]. Once the energy of the radiation approaches the Quantum Chromodynamics (QCD) confinement scale (~ 200–300 MeV), quarks and gluons will be directly emitted [17]. As they stream away from the BH, the quarks and gluons should fragment and hadronize (analogous to jets seen in high-energy collisions in terrestrial accelerators) into the particles which are stable on astrophysical timescales [3]. Thus in the SEM, the evaporating black hole is an astronomical burst of photons, neutrinos, electrons, positrons, protons and anti-protons (and for sufficiently nearby sources, neutrons and anti-neutrons [18,19]).

The purpose of this paper is to examine the observational characteristics of the final evaporation phase of a BH according to the SEM, incorporating the recent Large Hadron Collider (LHC) results for TeV energies, and to explore observational strategies that can be used in direct PBH burst searches, with particular relevance for the High Altitude Water Cherenkov (HAWC) observatory. Included is a discussion of the limitations and advantages of specific burst search methods and unique PBH burst signatures. In Section 2, we review the black hole Hawking radiation process. In Section 3, we use an empirical fragmentation function to calculate the BH photon spectrum and light curve and to parameterize the instantaneous photon emission from a BH burst. In Section 4, we explore methods for direct searches for PBH bursts and the procedures for setting upper limits on the PBH distribution which would arise from null detection. We also discuss how one can potentially differentiate a PBH burst from other known cosmological GRB sources. In Section 5, modifications that could arise from high energy physics beyond the Standard Model are elucidated. In Section 6, we discuss the applicability and limitations of various assumptions employed in our PBH burst properties calculations. A summary of our findings and conclusions is given in Section 7.

2. BH emission theory

2.1. Hawking radiation

Hawking showed that a black hole radiates each fundamental particle species at an emission rate of [2,20]

$$\frac{d^2N}{dEdt} = \frac{\Gamma/2\pi\hbar}{e^x - (-1)^{2s}}\, n_{\rm dof}, \tag{1}$$

where s is the particle spin, $n_{\rm dof}$ is the number of degrees of freedom of the particle species (e.g. spin, electric charge, flavor and color), Γ is the absorption coefficient, and $\hbar$ is the reduced Planck constant. The dimensionless quantity x is defined by

$$x \equiv \frac{8\pi GM_{BH}E}{\hbar c^3} = \frac{E}{kT_{BH}} \tag{2}$$

for a nonrotating, uncharged 4D black hole, where E is the energy of the Hawking-radiated particle, M_{BH} is the black hole mass, T_{BH} is the black hole temperature,

$$kT_{BH} = \frac{\hbar c^3}{8\pi GM_{BH}} = 1.058\left(\frac{10^{10}\ \text{kg}}{M_{BH}}\right)\ \text{GeV}, \tag{3}$$

G is the universal gravitational constant, c is the speed of light and k is Boltzmann's constant. Because initial black hole rotation and/or electric charge is radiated away faster than mass, we will assume a nonrotating, uncharged black hole in our analysis; extension to rotating and/or charged black holes is straightforward [17,21,22].

The absorption coefficient Γ depends on M_{BH}, E and s. For an emitted species of rest mass m, Γ at $E \gg mc^2$ has the form

$$\Gamma(M_{BH}, E, s) = 27\left(\frac{x}{8\pi}\right)^2 \gamma_s(x) \tag{4}$$

such that $\gamma_s(x) \to 1$ for large x. The functions $\gamma_s(x)$ are shown in Fig. 1 for massless or relativistic uncharged particles with $s = 0$, $s = 1/2$ and $s = 1$ [17,21–26]. For a non-relativistic $s = 1/2$ particle, Γ at $E = mc^2$ remains at least 50% of the relativistic value and, when $kT_{BH} \gtrsim 0.1mc^2$, only deviates noticeably from the relativistic value at $E \lesssim 2mc^2$ [22]. Below $E = mc^2$, $\Gamma = 0$. Electrostatic effects associated with the emission of a particle of electric charge e decrease Γ by at most a few percent [22].

Combining the above equations, the emission rate per fundamental particle species can be written in the form

$$\frac{d^2N}{dEdt} = \frac{27}{2\pi\hbar(8\pi)^2} n_{\rm dof}\psi_s(x) \tag{5}$$

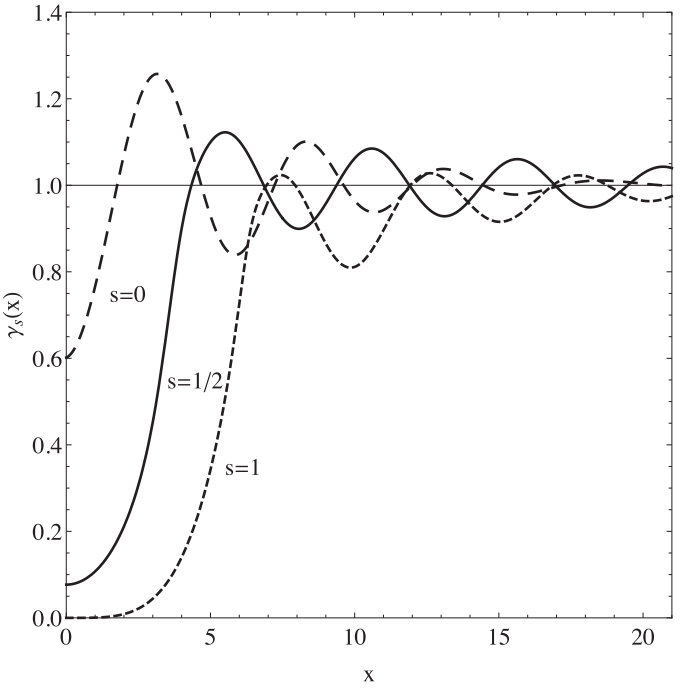

Fig. 1. The functions $\gamma_s(x)$ for massless spin-0 (long dashed line), spin-1/2 (solid line) and spin-1 (short dashed line) particles.

where

$$\psi_s(x) \equiv \frac{\gamma_s(x)x^2}{e^x - (-1)^{2s}}. \tag{6}$$

The dimensionless emission rate functions, $\psi_s(x)$, are plotted in Fig. 2 for $s = 0,\ 1/2$, and 0. The distribution $\psi_s(x)$ peaks at $x = x_{r,s}$ where $x_{r,s=0} = 2.19$ for uncharged massless or relativistic particles, $x_{r,s=1/2} = 4.02$ for relativistic particles with charge $\pm\ e$, and $x_{r,s=1} = 5.77$ for uncharged massless or relativistic particles [17,22–26]. The emission rate integrated over energy, per emitted fundamental species, is

$$\frac{dN}{dt} = \int_0^\infty \frac{d^2N}{dEdt}dE \tag{7}$$

$$= \frac{27c^3}{2\pi G(8\pi)^3 M_{BH}} n_{\rm dof}\Psi_s = \frac{1.093\times 10^{22}}{\left(M_{BH}/10^{10}\ {\rm kg}\right)} n_{\rm dof}\Psi_s\ {\rm s}^{-1} \tag{8}$$

$$= \frac{27kT_{BH}}{2\pi\hbar(8\pi)^2} n_{\rm dof}\Psi_s = 1.033\times 10^{22}\left(\frac{T_{BH}}{\rm GeV}\right) n_{\rm dof}\Psi_s\ {\rm s}^{-1} \tag{9}$$

where

$$\Psi_s \equiv \int_0^\infty \frac{\gamma_s(x)x^2}{e^x - (-1)^{2s}}dx. \tag{10}$$

Per degree of freedom, $\Psi_{s=0} = 2.45$ for uncharged massless or relativistic particles, $\Psi_{s=1/2} = 0.897$ for uncharged relativistic particles, $\Psi_{s=1/2} = 0.879$ for relativistic particles with charge $\pm e$, and $\Psi_{s=1} = 0.273$ for uncharged massless or relativistic particles [17,22–26].

Fig. 3 displays the direct radiation rates according to Eq. (1) for a single relativistic quark flavor ($n_{\rm dof} = 12$) and for gluons ($n_{\rm dof} = 16$), as functions of x. (In Fig. 3 we have neglected the electric charge of the quark which affects the quark emission rate by less than 5% [17,22].)

In order to calculate the spectrum of the final photon burst from the PBH, two important relations pertaining to the final phase of BH evaporation are needed. The first relation we require is the black hole mass M_{BH} as a function of time [23]

$$\frac{dM_{BH}}{dt} \equiv -\frac{\alpha(M_{BH})}{M_{BH}^2}, \tag{11}$$

where the function $\alpha(M_{BH})$ incorporates all directly emitted particle species and their degrees of freedom. As the BH evaporates, the value of M_{BH} is reduced by an amount equal to the total mass-energy of the emitted particles. By conservation of energy,

$$\frac{d(M_{BH}c^2)}{dt} = -\sum_i \int_0^\infty \frac{d^2N_i}{dEdt} EdE \tag{12}$$

where the summation over i is over all the fundamental species and so

$$\alpha(M_{BH}) = \frac{M_{BH}^2}{c^2}\sum_i \int_0^\infty \frac{d^2N_i}{dEdt} EdE. \tag{13}$$

Substituting for M_{BH} in terms of T_{BH} and E in terms of x, we can write

$$\alpha(M_{BH}) = \frac{27\hbar c^4}{2\pi G^2(8\pi)^4}\sum_i \int_0^\infty n_{\ {\rm dof},i}\phi_{s_i}(x)dx \tag{14}$$

where $\phi_s(x) \equiv \psi_s(x)x$.

The dimensionless emitted power functions, $\phi_s(x)$, are shown in Fig. 4 for $s = 0,\ 1/2$, and 0. The distribution $\phi_s(x)$, and hence the instantaneous power emitted in each fundamental state, peaks at $x = x_{p,s}$ where $x_{p,s=0} = 2.66$ for uncharged massless or relativistic particles, $x_{p,s=1/2} = 4.40$ for uncharged relativistic particles, $x_{p,s=1/2} = 4.53$ for relativistic particles with charge $\pm\ e$, and $x_{p,s=1} = 6.04$ uncharged massless or relativistic particles [17,22–26]. As the remaining BH evaporation lifetime τ decreases, T_{BH} increases and new fundamental quanta begin to contribute significantly to $\alpha(M_{BH})$ once T_{BH} crosses each relevant mass threshold, $kT_{BH} \sim m_ic^2/x_{p,s_i}$. At $kT_{BH} \gtrsim m_ic^2$, the contribution of a specific fundamental species i to $\alpha(M_{BH})$ is

$$\alpha_i = \frac{27\hbar c^4}{2\pi G^2(8\pi)^4} n_{\ {\rm dof},i}\Phi_{s_i} = 2.06\times 10^{15} n_{\ {\rm dof},i}\Phi_{s_i}\ {\rm kg^3 s^{-1}}, \tag{15}$$

where

$$\Phi_s = \int_0^\infty \frac{\gamma_s(x)x^3}{e^x - (-1)^{2s}}dx. \tag{16}$$

Per degree of freedom, $\Phi_{s=0} = 6.89$ for massless or relativistic particles, $\Phi_{s=1/2} = 3.79$ for uncharged relativistic particles, $\Phi_{s=1/2} = 3.68$ for relativistic particles with charge $\pm\ e$, and $\Phi_{s=1} = 1.56$ for massless or relativistic particles [17,22–26]. From the values for uncharged and $\pm\ e$-charged $s = 1/2$ modes, we can linearly interpolate approximate values for relativistic $\pm\ e/3$-charged d, s and b quarks ($\Phi_{s=1/2} \simeq 3.75$ per d, s or b degree of freedom) and for relativistic $\pm\ 2e/3$-charged u, c and t quarks ($\Phi_{s=1/2} \simeq 3.72$ per u, c or t degree of freedom).

Counting only the experimentally confirmed fundamental Standard Model particles [27], a $kT_{BH} \simeq 1$ GeV ($M_{BH} \simeq 10^{10}$ kg) black hole should directly emit the following field quanta: the three charged leptons ($s = 1/2,\ n_{dof} = 12$); the three neutrinos ($s = 1/2,\ n_{dof} = 6$) where we assume that the neutrinos are Majorana particles with negligible mass; five quark flavors ($s = 1/2,\ n_{dof} = 60$); the photon ($s = 1,\ n_{dof} = 2$); and the gluons ($s = 1,\ n_{dof} = 16$). This gives

$$\alpha(kT_{BH} \simeq 1\,{\rm GeV}) = 6.6\times 10^{17}\ {\rm kg^3\ s^{-1}}. \tag{17}$$

At $kT_{BH} \simeq 50$ GeV ($M_{BH} \simeq 2\times 10^8$ kg), the list also includes the top quark, the $W^\pm$ and Z^0 massive vector bosons ($s = 1,\ n_{dof} = 9$), and the Higgs boson ($s = 0,\ n_{dof} = 1$, and treating the Higgs boson as a 125 GeV resonance [28]). This gives

$$\alpha(kT_{BH} \simeq 50\,{\rm GeV}) = 8.0\times 10^{17}\ {\rm kg^3\ s^{-1}}. \tag{18}$$

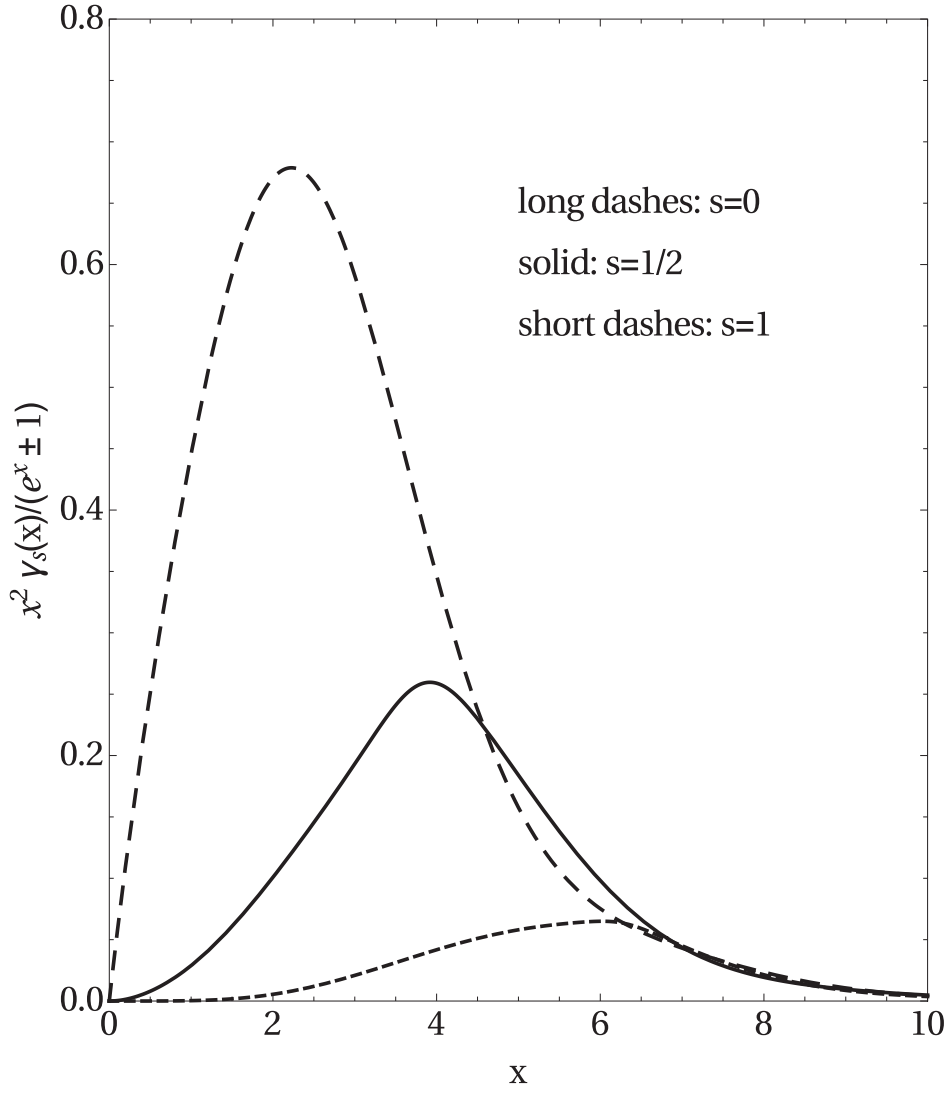

Fig. 2. The dimensionless emission rate per degree of freedom, $\psi_s(x) = x^2\gamma(x)/(e^x \pm 1)$ as a function of x for $s = 0$, 1/2, and 1.

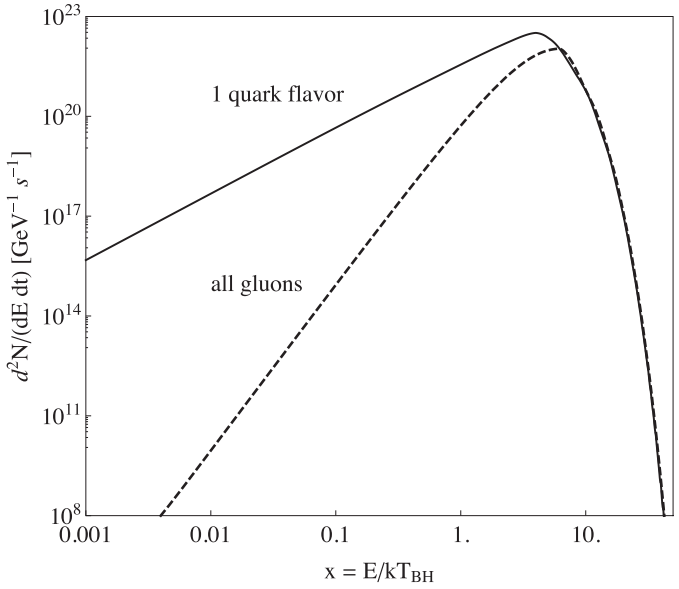

Fig. 3. Rates of Hawking radiation of a massless quark flavor and of gluons, as functions of x. For $x \ll 1$, the power laws are $\psi \propto x^2$ for $s = 1/2$ and $\psi \propto x^3$ for $s = 1$.

Energies well above the Higgs field vacuum expectation value ~246 GeV have not yet been explored in high energy accelerators. The ten fundamental modes of $W^{\pm}$, Z^0 and H^0 are expected to be counted differently above the electroweak symmetry breaking phase transition because of expected restoration of SU(2) × U(1) gauge symmetry [29], although this has yet to be confirmed in accelerator experiments. By the Goldstone Boson Equivalence Theorem, the longitudinal modes of the $W^{\pm}$ and Z^0 bosons observed at lower energies are expected to be expressed as scalar modes at these energies. In this case, there would be six transverse vector $s = 1$ fields and four scalar $s = 0$ fields of $W^{\pm}$, Z^0 and H^0, giving an the asymptotic value of $\alpha(M_{BH}) \simeq 8.3 \times 10^{17}$ kg^{3}s^{-1} for $kT_{BH} >$ 100 GeV ($M_{BH} < 10^8$ kg). Because this has not yet been observed experimentally and there are other possible arrangements at high energies, however, we will confine our modes to those which have been experimentally confirmed and use as our asymptotic value of

$$\alpha_{SM} = 8.0 \times 10^{17}\ \text{kg}^3\ \text{s}^{-1} \tag{19}$$

in subsequent calculations for $kT_{BH} > 100$ GeV ($M_{BH} < 10^8$ kg). We note that the ambiguity in counting $s = 0$ and $s = 1$ states as T_{BH} transitions through and above the electroweak symmetry breaking scale has a negligible effect on the BH emission spectra because of the dominance of the $s = 1/2$ modes at these T_{BH}.

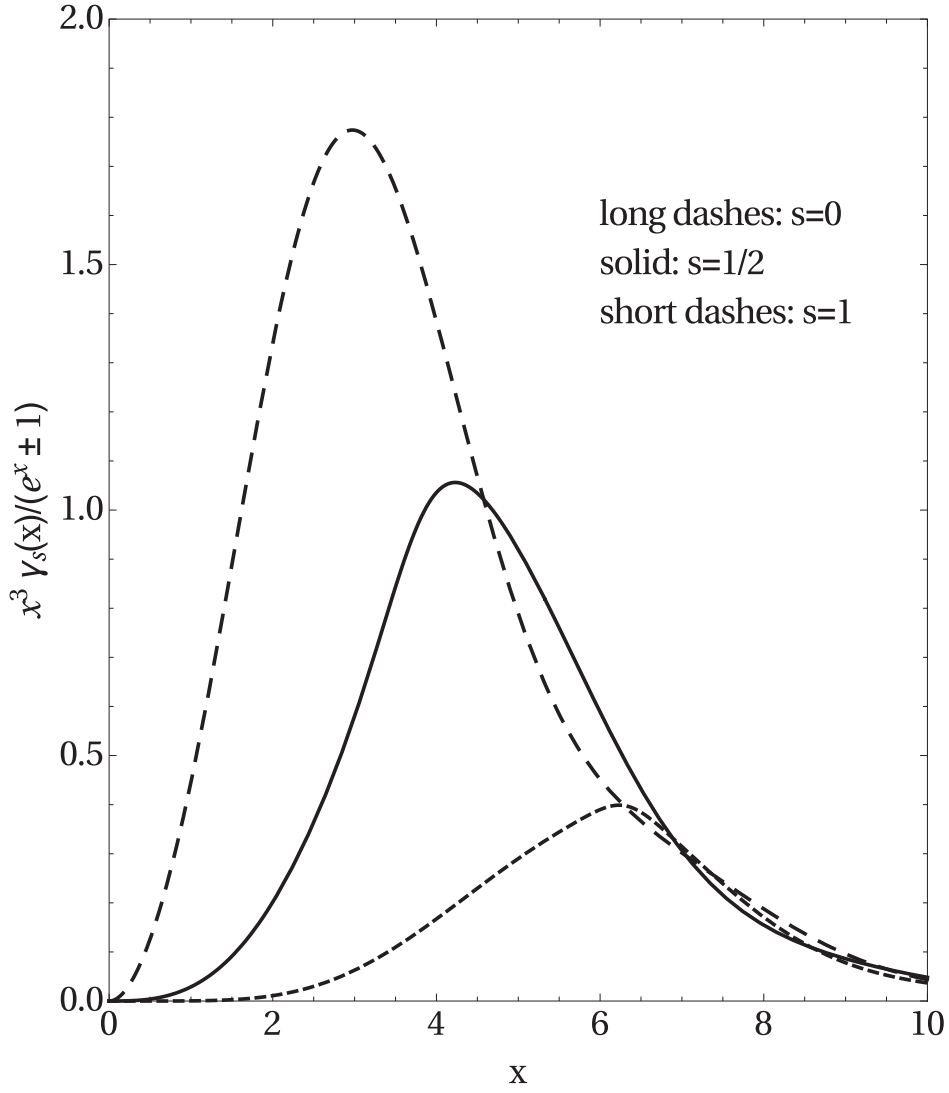

Fig. 4. The dimensionless emitted power per degree of freedom, $\phi_s(x) = x^3\gamma(x)/(e^x \pm 1)$ as a function of x for $s = 0,\ 1/2$, and 1.

Fig. 5 illustrates $\alpha(M_{BH})$ and $\alpha(T_{BH})$ for the SEM. In Fig. 5, the function is presented as piece-wise constant with each horizontal line segment representing the sum of the asymptotic contributions for $kT_{BH} > m_i c^2/x_{p,s_i}$. As the end of the BH's lifetime approaches, T_{BH} exceeds the rest masses of all known fundamental particles, and α reaches a constant asymptotic value, α_{SM}.

For the current and future generations of very high energy (VHE) gamma-ray observatories, we are interested in bursts generated by black holes of temperature $kT_{BH} \gtrsim 1$ TeV. For $kT_{BH} \gtrsim 1$ TeV (corresponding to $M_{BH} \lesssim 10^7$ kg and a remaining evaporation lifetime of $\tau \lesssim 500$ s), we have $\alpha(M_{BH}) \approx \alpha_{\rm SM}$. Returning to Eq. (11), the BH mass as a function of remaining evaporation lifetime τ in this regime is then

$$M_{BH}(\tau) \approx (3\alpha_{\rm SM}\,\tau)^{1/3} = 1.3 \times 10^6 \left(\frac{\tau}{1s}\right)^{1/3} \ \text{kg}. \tag{20}$$

The second relation we require is the BH temperature T_{BH} expressed as a function of τ for the final evaporation phase. Combining Eq. (3) and Eq. (20), we have for $kT_{BH} \gtrsim 1$ TeV

$$kT_{BH} = 7.8 \left(\frac{\tau}{1s}\right)^{-1/3} \ \text{TeV} \tag{21}$$

$$\tau = 4.8 \times 10^2 \left(\frac{kT_{BH}}{\text{TeV}}\right)^{-3} \ \text{s}. \tag{22}$$

Strictly, the above equations apply provided that the black hole temperature is below the Planck temperature $T_{\rm Pl}$ ($\simeq 1.22 \times 10^{16}$ TeV). However, because the remaining evaporation lifetime dramatically shortens as T_{BH} increases, the behavior of the BH close to $T_{\rm Pl}$ has negligible effect on the astronomically observable emission spectra.

The black hole mass and temperature for the final 100 s of evaporation lifetime, corresponding to temperatures $kT_{BH} \gtrsim 2$ TeV, are shown in Fig. 6. VHE gamma-ray observatories are sensitive to photon energies in the range from ~50 GeV to 100 TeV. Thus the relevant x range for the final 100 s of the PBH burst is $0 \lesssim x \lesssim 50$. The instantaneous emission rates for a relativistic quark flavor and for gluons as a function of x in this range is included in Fig. 3.

In order to elucidate the behavior near the end of the black hole's evaporation lifetime, we now investigate the emission rate and spectrum as functions of τ. Fig. 7 shows the instantaneous emission rate $d^2N/(dEdt)$ for a relativistic or massless quark flavor, as a function of quark energy E, when $\tau = 100,\ 10,\ 1,\ 0.1,\ 0.01$ and 0.001 s. As $\tau \to 0$ and T_{BH} increases, the emission rate per directly Hawking-radiated $s = 1/2$ degree of freedom is constant at the peak but increases at high energies and decreases at low energies because the location of the peak scales with T_{BH}.

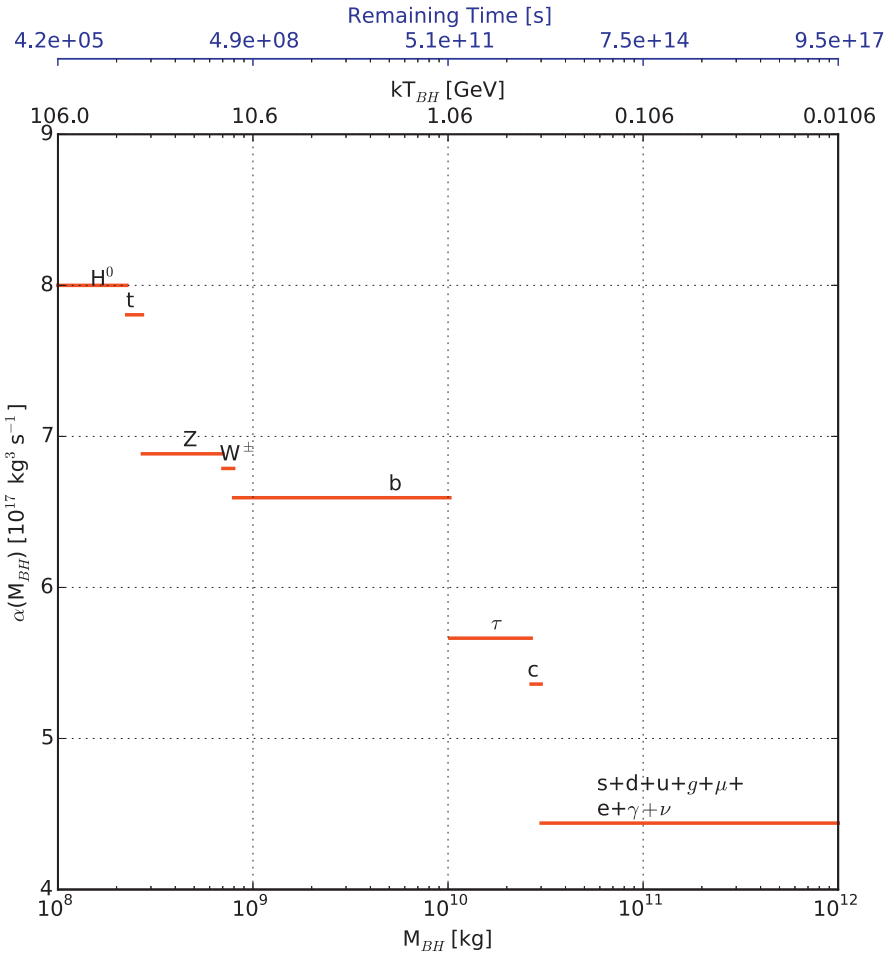

Fig. 5. The function $\alpha(M_{BH})$ in the Standard Evaporation Model. The asymptotic value for the SEM is 8.0×10^{17} kg^3 s^{-1}.

The SEM theory of Hawking radiation in the final 100 s has only one parameter with physical dimensions, which may be taken to be kT_{BH}. Because $kT_{BH} \gtrsim 2$ TeV is much larger than any Standard Model particle rest mass, all Hawking-radiated particles may be approximated as ultra-relativistic. Thus the $kT_{BH} \gtrsim 2$ TeV instantaneous emission rate per fundamental particle species depends essentially only on the ratio $x = E/kT_{BH}$, as in Fig. 3: the dependence of the rate on E is the same for different τ values except for a translation proportional to T_{BH} (see Fig. 7) and the SEM Hawking radiation rate per degree of freedom has a scale invariance with respect to x.

This scale invariance leads to useful power law approximations. For example, the direct Hawking emission rate for Dirac particles with $x \ll 1$ is proportional to x^2 (recall Fig. 3) and the direct Hawking emission rate for vector $s = 1$ particles with $x \ll 1$ is proportional to x^3 [23]. Other power laws appear in the emission rate for the final state photons that are created in the decays of the directly Hawking-radiated quarks and gluons.

2.2. QCD fragmentation

According to the SEM, Eq. (1) applies to the direct Hawking radiation of the fundamental particles of the Standard Model of high-energy physics: the leptons, quarks, and the gauge bosons [2,17,20,23,30]. As they stream away from the BH, these fundamental particles will then evolve by Standard Model processes, into the particles which are stable on astrophysical timescales. In particular, quarks and gluons will undergo fragmentation and hadronization into intermediate states which will eventually decay into photons, neutrinos, electrons, positrons, protons and anti-protons. Because the mean lifetime of a neutron at rest is $\sim 10^3$ s, undecayed neutrons of high energy E_N should also arrive from PBHs closer than $\sim (E_N/100 \text{ TeV})$ pc.

For application to PBH searches at VHE gamma-ray observatories, we seek the total photon emission rate from the BH. The photon production has several components[4]: (i) The "direct photons" produced by the direct Hawking radiation of photons: this component peaks at a few times T_{BH} and is most important at the highest photon energies at any given T_{BH}. (ii) The "fragmentation photons" arising from the fragmentation and hadronization of the quarks and gluons which are directly Hawking-radiated by the BH (in particular, quark and gluon fragmentation and hadronization generates π^0's which decay into two photons with a branching fraction of 98.8%): this component is the dominant source of photons at energies below T_{BH}. (iii) The photons produced by the decays of other Hawking-radiated fundamental particles, e.g., the tau lepton, W and Z gauge bosons, and Higgs boson; this component is small compared to the component produced by the fragmentation of directly Hawking-radiated quarks and gluons and is neglected here. (We note that because the W, Z, and Higgs bosons decay predominantly via hadronic channels, their main effect is to enhance the fragmentation photon component by at most ~10%.)

[4] Because we are investigating photon energies $\gtrsim 50$ GeV, we do not include the white inner bremsstrahlung photon component generated by the Hawking radiation of charged fermions which is dominated at these energies by the fragmentation photons [31].

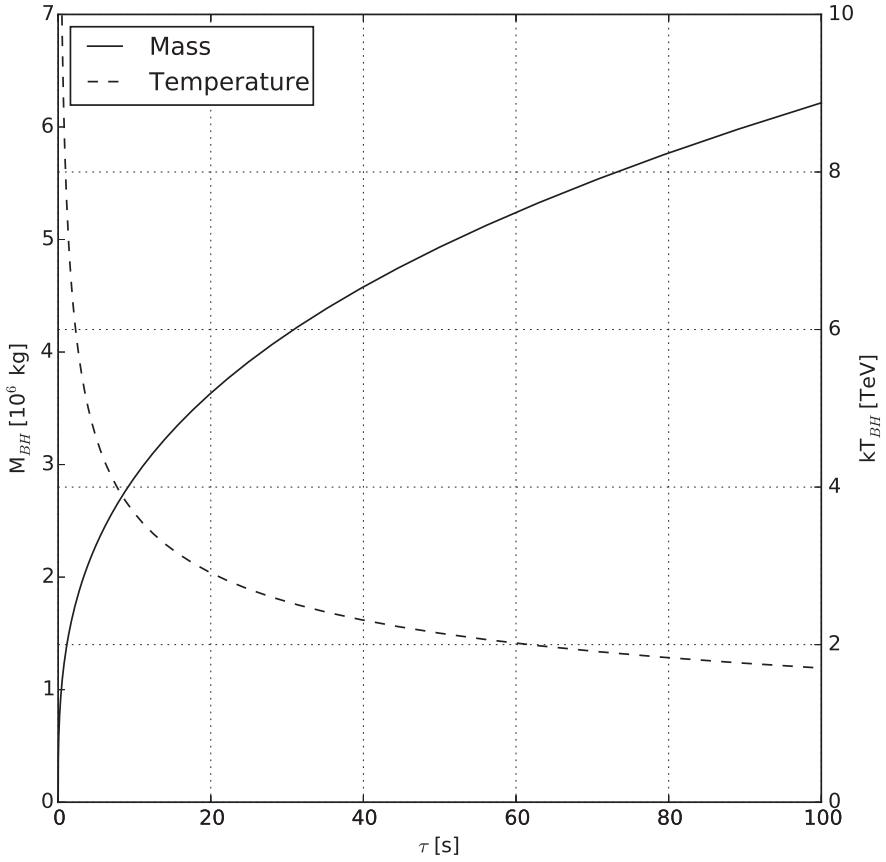

Fig. 6. Black hole mass and temperature for the final 100 s of the BH evaporation lifetime (τ is the remaining time). The decrease of mass and the increase of temperature accelerate as $\tau \to 0$.

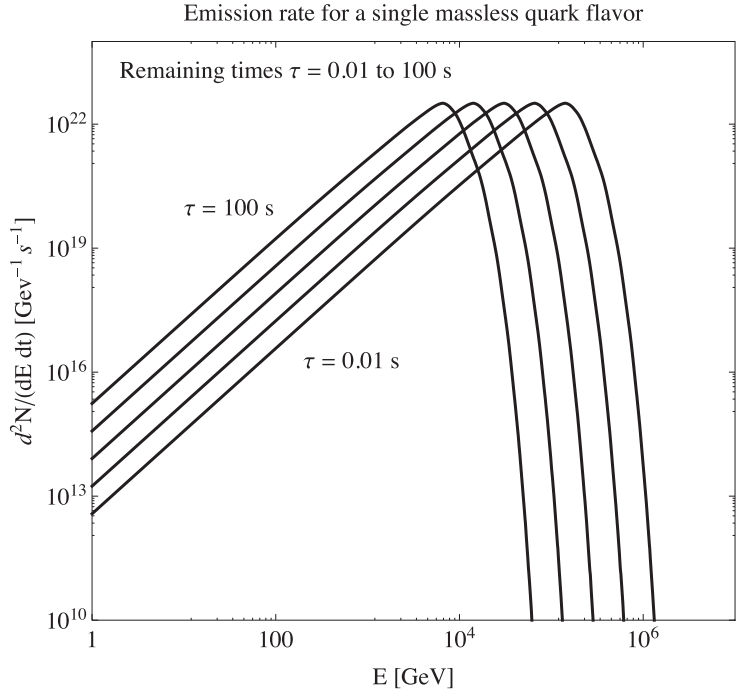

Fig. 7. Instantaneous number emission rate for a single massless quark flavor, as a function of quark energy E, at five values of remaining evaporation lifetime τ: 100, 10, 1, 0.1, 0.01 s.

In the SEM, the production rate of hadrons by the BH is equal to the integrated convolution of the Hawking emission rates for the relevant fundamental particles i (Eq. (1)) with fragmentation functions $D_{h/i}(z)$ describing the fragmentation of species i into hadron h, where $z = E_h/E$ is the fraction of the initial particle's energy E carried by the hadron; i.e.,

$$\frac{d^2N_h}{dE_h dt} = \sum_i \int_{m_h c^2}^{\infty} \int_0^1 \frac{d^2N_i}{dE dt}\, D_{h/i}(z)\, \delta(E_h - zE)\, dz\, dE. \tag{23}$$

Here the summation is over all contributing fundamental species i and $D_{h/i}(z)dz$ is the number of hadrons h with energy fraction in the range from z to $z + dz$ produced by the fragmentation of fundamental particle i.

For the current study, we wish to describe the photon burst generated in the final moments of the BH's evaporation lifetime and the resulting light curve and energy spectrum seen by the detector. Fragmentation functions $D_{b/a}(z)$ have been measured in high-energy physics experiments, such as e^+e^- annihilation, for a variety of initial partons (a) and final fragments (b) [32,33]. However, a complete set of fragmentation functions is not available. We turn therefore to a simplified fragmentation model. This model, which has appeared in the literature previously to estimate the photons derived from the fragmentation of partons [4,34,35], is expected to provide a realistic representation of the photon spectrum for our purpose and has been used in the analyses of PBH searches by several gamma-ray observatories [7,9]. Alternatively, Eq. (23) can be evaluated using a Monte Carlo simulation which incorporates a parton showering program such as Pythia [36] or Herwig [37] extended to generate decays into the astrophysically stable species, including photons. This approach has also previously been used in PBH flux calculations [17] and is necessary if the goal is to obtain full spectral details about the instantaneous flux of final-state particle species. We note that in both approaches, the $kT_{BH} \gtrsim 2$ TeV BH burst calculation requires extrapolation of the fragmentation functions or event generator codes to higher energies than have been validated in accelerator experiments.

3. Photons from a BH burst

3.1. The pion fragmentation model

For photon production, the most important decay from the fragmentation of the initial quark or gluon is $\pi^0 \to 2\gamma$. In the pion fragmentation model, we proceed assuming that the QCD fragmentation of quarks and gluons may be approximated entirely by the production of pions. Two questions must be addressed by the model: what is the pion spectrum generated by the partons and what is the photon spectrum generated by the pion decays?

To answer the first question, we utilize a heuristic fragmentation function

$$D_{\pi/i}(z) = \frac{15}{16}\, z^{-3/2}\, (1-z)^2 \tag{24}$$

where $z \equiv E_\pi/E$ is the energy fraction carried by a pion generated by a parton of energy E [4,34,35]. This function is normalized such that $\int_0^1 z D_{\pi/i}(z)dz = 1$; i.e., all of the initial parton energy is converted to go into pions. Fig. 8 shows the fragmentation function $D_{\pi/i}(z)$. The results in this paper are based on assuming the pion fragmentation function $D_{\pi/i}(z)$ of Eq. (24) for all initial Hawking-radiated quarks and gluons. We note, though, that the function Eq. (24) implies an average energy for the final state photons and a multiplicity (number) of final state photons per initial parton which match the $T_{BH}^{1/2}$ scaling of the photon average energy and multiplicity found using a HERWIG-based Monte Carlo simulation to generate fragmentation and hadronization of the Hawking-radiated particles from 1 GeV $\leq T_{BH} \leq$ 100 GeV black holes [17]. We discuss the accuracy of this heuristic model further in Section 6.1.[5]

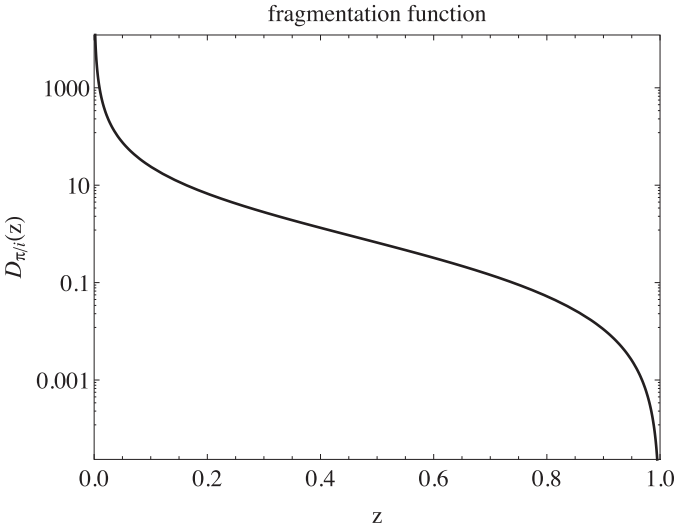

Fig. 8. The heuristic fragmentation function $D_{\pi/i}(z)$ as a function of the pion energy fraction, z.

The instantaneous pion production rate by the BH is then

$$\frac{d^2N_\pi}{dE_\pi dt} = \sum_i \int_{m_\pi c^2}^{\infty} \int_0^1 \frac{d^2N_i}{dE_i dt}\, D_{\pi/i}(z')\, \delta(E_\pi - z'E_i) dz' dE_i. \tag{25}$$

Fig. 9 shows the instantaneous pion rate as a function of $x_\pi \equiv E_\pi/kT_{BH}$. At high pion energies, the pion rest mass is negligible and this function has a scaling form: it depends only on the dimensionless ratio x_π. (Similarly, we saw that the quark and gluon rates depend only on $x = E/kT_{BH}$ when T_{BH} is large compared to the quark masses.) Comparing Fig. 3 and Fig. 9 elucidates how the fragmentation of quarks and gluons at high energies, say $E >$ 10–100 TeV, yields a significant flux of pions at lower energies, say 1 GeV $< E_\pi <$ 100 TeV; the π^0 decays then produce photons in the detectable energy range of VHE gamma-ray observatories.

We assume that the pions are generated by the fragmentation and hadronization of the 72 directly Hawking-radiated $s = 1/2$ quark modes[6] and the 16 directly Hawking-radiated $s = 1$ gluon modes. The directly Hawking-radiated $W^\pm$ and Z^0 bosons also decay via hadronic jets about 70% of the time. Because $W^\pm$ and Z^0 are expected to each have only two polarization states when $kT_{BH} \gtrsim 1$ TeV (giving a total of six fundamental degrees of freedom) and $\Psi_{s=1/2} \simeq 3\Psi_{s=1}$, however, the Hawking-radiated $W^\pm$ and Z^0 increase the instantaneous pion production rate of Fig. 7 by only ~3%.

Higgs modes also contribute to the pion flux to a small extent. The dominant decay modes for the experimentally-confirmed H^0 resonance at 125 GeV are $H^0 \to b + \bar{b}$ and $H^0 \to W^+ + W^-$. The dominant decay modes of any other Higgs states (which have not yet been discovered) are also expected to be $H \to q + \bar{q}$ and decays via $W^\pm$ and Z^0 bosons. Noting that $\Psi_{s=0} \simeq 2\Psi_{s=1/2}$, the directly Hawking-radiated Higgs boson states can increase the instantaneous pion production rate of Fig. 9 by at most ~10%.

[5] The function $D_{\pi/i}(z)$ resembles closely the result of a QCD calculation [34] which has been used for theoretical calculations in a previous PBH search [9]. Section 6.1 has a discussion of the heuristic fragmentation function $D_{\pi/i}(z)$, compared to empirical fragmentation functions that have been extracted from collider data.

[6] Quarks come in six flavors, three colors, two spin states, and as particles or antiparticles for a total of 72 modes.

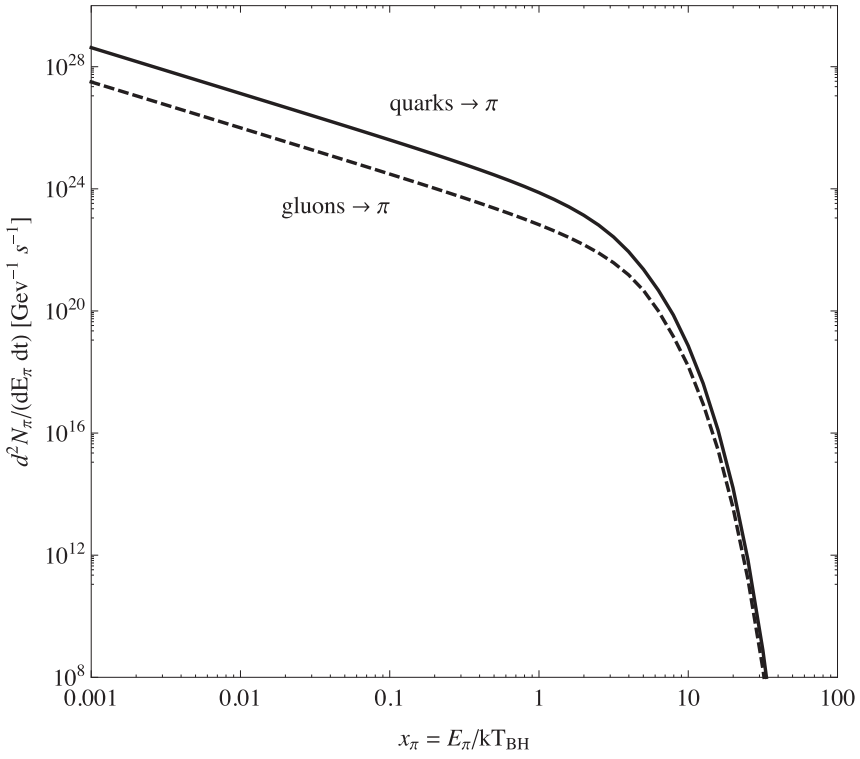

Fig. 9. The pion production rate $d^2N_\pi/(dE_\pi\,dt)$ calculated from Eq. (25), plotted as a function of $x_\pi = E_\pi/kT_{BH}$. The number of degrees of freedom is $n_{dof} = 72$ for quarks and $n_{dof} = 16$ for gluons. The quark contribution is dominant. For $x_\pi < 1$ the particle rate obeys a power law: $d^2N_\pi/(dE_\pi\,dt) \propto x_\pi^{-3/2}$. The power index of $-3/2$ matches the low-z behavior of the assumed fragmentation function, which varies as $z^{-3/2}$.

3.2. Photon flux from pion fragmentation

We now obtain the photon flux from the $\pi^0 \to 2\gamma$ decay of the pion distribution. Because the fragmentation function $D_{\pi/i}(z)$ includes all three pion charge states π^+, π^-, and π^0 as equal components,[7] and each π^0 decays into two photons, we must multiply by 2/3 to get the γ multiplicity. In the π^0 rest frame, the two photons have equal but opposite momenta and equal energies, $m_\pi c^2/2$. In the reference frame of the gamma-ray observatory detector, the energies of the two photons, E_γ, are unequal but complementary fractions of the π^0 energy in the detector frame, E_π. We assume that only one of the photons in each pair is detectable.[8]

Let θ be the angle between the momentum of the observed photon in the π^0 rest frame and the π^0 momentum in the detector frame. In the detector frame, $E_\gamma = (E_\pi/2)(1+\beta\cos\theta)$ where the π^0 velocity $\beta = v/c \approx 1$ and $E_\pi = m_\pi/\sqrt{1-\beta^2}$. Because the angular distribution of the photons is isotropic in the π^0 rest frame, the distribution of pion-produced photons in the detector frame is

$$\left(\frac{d^2N_\gamma}{dE_\gamma\,dt}\right)_{\text{frag.}} = \frac{2}{3}\int_{-1}^{1}\frac{2\pi\,d\cos\theta}{4\pi} \times \int_{m_\pi}^{\infty}\frac{d^2N_\pi}{dE_\pi\,dt}\delta[E_\gamma - (E_\pi/2)(1+\beta\cos\theta)]dE_\pi\,. \tag{26}$$

Evaluating the integral over $\cos\theta$, we have

$$\left(\frac{d^2N_\gamma}{dE_\gamma\,dt}\right)_{\text{frag.}} = \frac{2}{3}\int_{E_{\min}}^{\infty}\frac{d^2N_\pi}{dE_\pi\,dt}\frac{dE_\pi}{\sqrt{E_\pi^2 - m_\pi^2}}. \tag{27}$$

For $E_\gamma > m_\pi/4$, the minimum pion energy is $E_{\min} = E_\gamma + m_\pi^2/(4E_\gamma)$. Eq. (27) implies that the photon energy in the detector frame is uniformly distributed in the range

$$\frac{E_\pi(1-\beta)}{2} \le E_\gamma \le \frac{E_\pi(1+\beta)}{2}. \tag{28}$$

For high energy photons, we may approximate $m_\pi \approx 0$. In this case, the pion fragmentation function of Eq. (24) evolves into the photon distribution per initial parton

$$D_{\gamma/i}(z_\gamma) = \frac{15}{16}\left(\frac{16}{3} + \frac{2}{3}z_\gamma^{-3/2} - 4z_\gamma^{-1/2} - 2z_\gamma^{1/2}\right) \tag{29}$$

where $z_\gamma \equiv E_\gamma/E$ is the energy fraction carried by a photon generated by a parton of energy E.

Fig. 10 shows the instantaneous photon spectrum, including the directly Hawking-radiated photons, emitted by the black hole when the remaining BH evaporation lifetime is $\tau = 100,\ 10,\ 1,\ 0.1$ and 0.01 s.

3.3. Parameterization of the Black Hole photon spectrum

To simplify subsequent calculations, we parameterize the function for the fragmentation component of the total photon emission rate from the BH as follows. This parameterization is valid for $E_\gamma \gtrsim 1$ GeV.

By the scale invariance at short remaining time τ, $d^2N_\gamma/(dE_\gamma\,dt)$ depends on the ratio

$$x_\gamma = \frac{E_\gamma}{kT_{BH}(\tau)} = 1.287\times10^{-4}\left(\frac{E_\gamma}{1\ \text{GeV}}\right)\left(\frac{\tau}{1\ \text{s}}\right)^{1/3}. \tag{30}$$

[7] The charged pions do not contribute to the photon flux. However, they do yield neutrinos. The same heuristic model can be used to estimate the flux of neutrinos from the BH.

[8] The angle between the two photon trajectories in the detector frame will be very small because of the large Lorentz boost. However, if the BH is at a distance of order 1 pc from the detector, then only one of the photons from each π^0 decay will hit the detector.

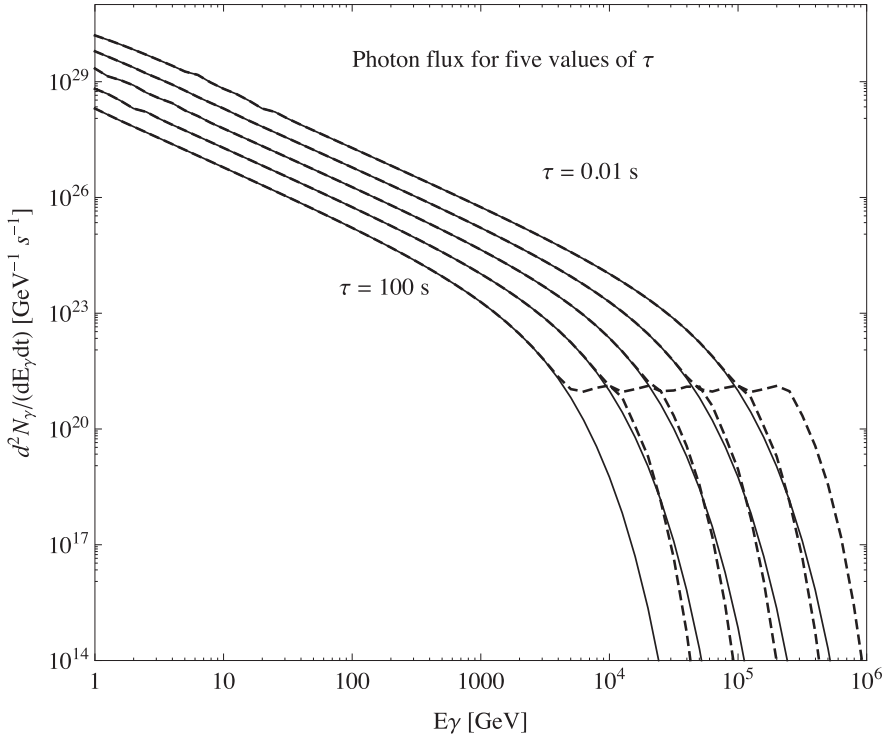

Fig. 10. The instantaneous photon emission rate $d^2N_\gamma/(dE_\gamma dt)$ for five values of the remaining BH burst lifetime, τ = 100, 10, 1, 0.1, and 0.01 s. The dashed curves show the total (fragmentation + direct) gamma-ray emission rate; the solid curves show the fragmentation only rate. As τ decreases, the rate increases.

Fitting the curve shown in Fig. 10, we derive a reasonable parameterization of the fragmentation contribution to be

$$\left(\frac{d^2N_\gamma}{dE_\gamma dt}\right)_{\text{frag.}} = Ax_\gamma{}^{-3/2}\left[1-\Theta_S(x_\gamma-0.3)\right] \tag{31}$$

$$+B\exp(-x_\gamma)[x_\gamma(x_\gamma+1)]^{-1}\Theta_S(x_\gamma-0.3) \tag{32}$$

where

$$A = 6.339\times10^{23}\ \text{GeV}^{-1}\ \text{s}^{-1}, B = 1.1367\times10^{24}\ \text{GeV}^{-1}\ \text{s}^{-1} \tag{33}$$

and

$$\Theta_S(u) = 0.5(1+\tanh(10u)). \tag{34}$$

The accuracy of this parameterization is ± 15% for $0.1 \le x_\gamma \le 10$, and ± 3% for smaller and larger x_γ. This is sufficient for most of our purposes. If greater accuracy is required, a table of the ratios of the approximate value to the exact value is used to correct the parameterized value.

We also derive, by curve-fitting, a parameterization of the directly Hawking-radiated photon component to be

$$\left(\frac{d^2N_\gamma}{dE_\gamma dt}\right)_{\text{direct}} = \frac{(1.13\times10^{19}\ \text{GeV}^{-1}\ \text{s}^{-1})(x_\gamma)^6}{\exp(x_\gamma)-1}F(x_\gamma) \tag{35}$$

where

$$F(x_\gamma) = 1.0 \quad \text{for } x_\gamma \le 2 \tag{36}$$

and

$$F(x_\gamma) = \exp\left\{\left[-0.0962-1.982\left(\ln x_\gamma-1.908\right)\right]\times\left[1+\tanh(20(\ln x_\gamma-1.908))\right]\right\} \text{ for } x_\gamma > 2. \tag{37}$$

An alternative parameterization of the total photon emission rate by Linton et al. [9], which has often been used in PBH searches by high-energy observatories, is

$$\frac{d^2N_\gamma}{dE_\gamma dt} = 6.24\times10^{23}\left[\frac{1}{8}\left(\frac{Q}{E_\gamma}\right)^{3/2}-\frac{3}{4}\sqrt{\frac{Q}{E_\gamma}}-\frac{3}{8}\sqrt{\frac{E_\gamma}{Q}}+1\right]\times\text{GeV}^{-1}\text{s}^{-1}, \quad \text{for} \quad E_\gamma < Q \tag{38}$$

$$\frac{d^2N_\gamma}{dE_\gamma dt} = 10^{21}\left(\frac{Q}{E_\gamma}\right)^4\ \text{GeV}^{-1}\text{s}^{-1}, \quad \text{for} \quad E_\gamma \ge Q \tag{39}$$

where $Q \simeq 4\times10^4(\tau/1\ \text{s})^{-1/3}$ GeV is the energy of the peak quark flux averaged over the last τ seconds of the PBH's evaporation lifetime [4]. The Linton et al. parameterization was derived by performing the convolution of Eq. (25) with an approximation to the quark emission rate which replaces the energy dependence of Fig. 7 with a delta function at Q. Eq. (38) is reasonably accurate for low energies but, for $E_\gamma > 0.1Q$, differences of up to 30% appear. More seriously, at $E_\gamma = Q$, the functional form of Eq. (38) drops to zero, which is not the actual behavior. Eq. (39) matches the photon emission rate reasonably to within 20% for $Q \le E_\gamma < 2Q$ but strongly overestimates the exponential fall off in the emission rate at the highest energies.

3.4. The time-integrated photon spectrum

In Section 3 we consider strategies for direct PBH burst searches at VHE gamma-ray observatories. One strategy is to utilize the photon time-integrated energy spectrum, i.e., the instantaneous photon emission rate integrated over a time interval from an initial remaining evaporation lifetime $t = \tau$ to the completion of evaporation at $t = 0$, as a function of energy,

$$\left[\frac{dN_\gamma}{dE_\gamma}\right]_\tau = \int_0^\tau \frac{d^2N_\gamma}{dE_\gamma dt}\,dt. \tag{40}$$

Fig. 11 shows the photon time-integrated energy spectra for τ = 0.01, 0.1, 1.0, 10.0, and 100.0 s using our parameterizations

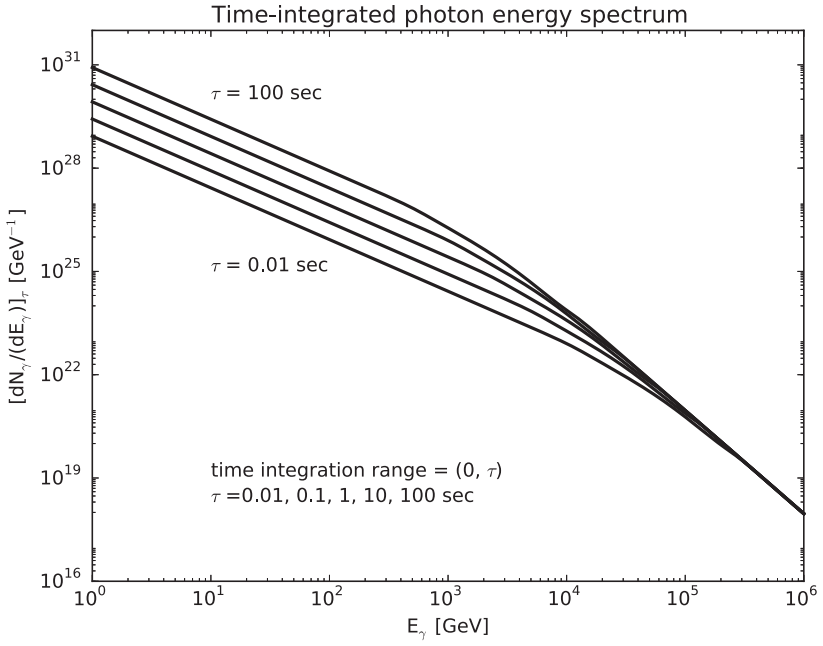

Fig. 11. The photon spectrum, integrated over the final BH evaporation lifetime intervals $\tau = 100, 10, 1, 0.1$ and 0.01 s.

of Section 3.3. In Fig. 11, it can be seen that $[dN_\gamma/dE_\gamma]_\tau$ obeys different power laws above and below a transition energy $E_{\rm tr}(\tau)$ which is of order $kT_{BH}(\tau)$: for $E_\gamma < E_{\rm tr}$, $\left[dN_\gamma/dE_\gamma\right]_\tau \propto E_\gamma^{-1.5}$ and for $E_\gamma > E_{\rm tr}$, $\left[dN_\gamma/dE_\gamma\right]_\tau \propto E_\gamma^{-3.0}$.

To understand the origin of these slopes, we first change the variable of the integration in Eq. (40) from t to $x(t) = E/kT_{BH}(t)$ where $kT_{BH}(t) = E_0(\tau_0/t)^{1/3}$ is given by Eq. (21) with $E_0 = 7800$ GeV and $\tau_0 = 1$ s. Thus $dt = 3\tau_0(E_0/E)^3x^2dx$ and

$$\left[\frac{dN_\gamma}{dE}\right]_\tau = 3\tau_0\left(\frac{E_0}{E}\right)^3\int_0^{x(\tau)}\psi_\gamma(x'_\pi)\,x'^2dx' \tag{41}$$

for a directly Hawking-radiated species. The integral in Eq. (40) is dominated at high E_γ by the directly Hawking-radiated photons and so Eq. (41) implies $[dN_\gamma/dE_\gamma]_\tau \sim E_\gamma^{-3}$ for high E_γ; this result reflects the fact that approximately $\tau \propto T_{BH}^{-3}$. The integral in Eq. (40) is dominated below $E_\gamma \sim kT_{BH}$ by the fragmentation function which must be convolved with Eq. (41) and gives $[dN_\gamma/dE_\gamma]_\tau \sim E_\gamma^{-3/2}$ for $E_\gamma \lesssim kT_{BH}$; this result reflects the fact that the fragmentation function Eq. (29) behaves as $z_\gamma^{-3/2}$ for $z_\gamma \to 0$.

A parameterization for the time-integrated photon spectrum, derived by fitting the HERWIG-based Monte Carlo simulations of the photon flux from 1 GeV $\le T_{BH} \le$ 100 GeV black holes of reference [17], was published by Bugaev et al. [38,39],

$$\frac{dN_\gamma}{dE_\gamma} \approx 9\times10^{35}\begin{cases}\left(\frac{1\ \text{GeV}}{T_\tau}\right)^{3/2}\left(\frac{1\ \text{GeV}}{E_\gamma}\right)^{3/2}\ \text{GeV}^{-1} & \text{for } E_\gamma < kT_\tau\\ \left(\frac{1\ \text{GeV}}{E_\gamma}\right)^{3}\ \text{GeV}^{-1} & \text{for } E_\gamma \ge kT_\tau\end{cases} \tag{42}$$

for $E_\gamma \gtrsim 1$ GeV. Here T_τ is the temperature of the black hole at the beginning of the final burst time interval, i.e., $T_\tau = T_{BH}(\tau)$ as given by Eq. (21). This approximation agrees well with our calculations of the time-integrated spectrum based on the pion fragmentation model, Eq. (24), and shown in Fig. 11. Either could be used as input for comparing the experimental sensitivities of different VHE gamma-ray observatories to a time-integrated PBH signal.

3.5. BH burst light curve

We now consider the time dependence of the BH burst, i.e., the final "chirp". In Section 4, we explore whether knowledge of the time dependence can be used to enhance statistical significance in a PBH search.

To find the time evolution of the BH burst, we integrate the differential emission rate $d^2N_\gamma/(dE_\gamma dt)$ over photon energy E_γ while retaining the time dependence. Hence the burst emission time profile (at the source) is

$$\left[\frac{dN_\gamma}{dt}\right]_{\rm Emission} = \int_{E_{\rm min}}^{E_{\rm max}}\frac{d^2N_\gamma}{dE_\gamma dt}dE_\gamma. \tag{43}$$

In general $E_{\rm min}$ and $E_{\rm max}$ are set by the energy range of the detector. Fig. 12 shows the BH burst emission time profile in the energy range 50 GeV $\le E_\gamma \le$ 100 TeV.

It is interesting to relate the photon time profile to the total luminosity function of the BH. By basic thermodynamics, the luminosity $dE/dt \propto T_{BH}^4 4\pi R^2$ per emitted mode. For a Schwarzschild black hole, the radius $R \propto M_{BH}$ and $T_{BH} \propto 1/M_{BH}$, and so $dE/dt \propto T_{BH}^2$ for the directly Hawking-radiated particles. Because the average energy of the directly Hawking-radiated particles is $\bar{E} \propto T_{BH}$, we expect for the directly Hawking-radiated particles that $dN/dt \sim \bar{E}^{-1}dE/dt \propto T_{BH}$. To estimate the τ dependence of dN_γ/dt, we note that the photon emission spectrum is dominated by the fragmentation component. The fragmentation function Eq. (24) implies a multiplicity (number of final states per initial particle) proportional to $T_{BH}^{1/2}$. Convolving the multiplicity dependence with the dN/dt dependence per Hawking-radiated state leads to $dN_\gamma/dt \propto T_{BH}^{3/2} \propto \tau^{-1/2}$, in agreement with the power law of approximately -0.5 found in Fig. 12. We also note that, because energy is conserved in the fragmentation and hadronization process, the total BH luminosity summed over all final state species is approximately $dE/dt \propto \tau^{-2/3}$.

The dependence of the BH burst emission time profile on the energy range ($E_{\rm min}$, $E_{\rm max}$) is also relevant. Fig. 13 shows dN_γ/dt calculated using several ($E_{\rm min}$, $E_{\rm max}$) energy bands between 0.1 GeV and 1000 TeV. We see that the low energy bands between 0.1 GeV and 10 TeV have similar emission profiles. However, above energies

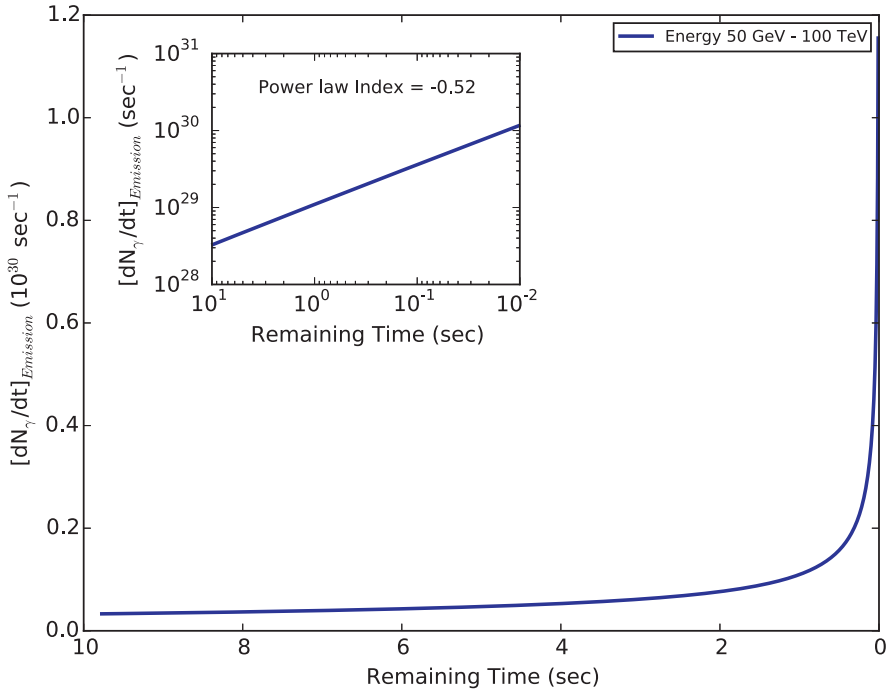

Fig. 12. The BH burst emission time profile, the emission rate integrated over energy, for the energy range 50 GeV–100 TeV. As discussed in the text, this shape is well described by a power law with an index of ~ -0.5.

of $\sim$10 TeV the burst emission time profile is energy-dependent and has an inflection region occurring $\sim$1 s to 0.1 s before the end of the BH evaporation lifetime. This energy dependence can be seen in the bottom panel of Fig. 13, where we have plotted several energy bands above 10 TeV. The energy dependence of the burst emission time profile can be understood by referring to Eqs. (31) and (35) and Fig. 10. At low energies (below the inflection region), the photons generated by the Hawking-radiated quarks and gluons dominate the flux; at high energies (above the inflection point), the directly Hawking-radiated photons dominate the flux. In the inflection region, the two components are comparable.

Figs. 12 and 13 display the emission time profiles, i.e., the source emission rate as a function of remaining time. Let us now consider the detection time profile, i.e., the *light curve* of the PBH burst for a specific VHE gamma-ray observatory. The detection time profile can be calculated from

$$\left[\frac{dN_\gamma}{dt}\right]_{\text{Detection}} = \frac{1}{4\pi r^2}\int_{E_{\min}}^{E_{\max}} A(E_\gamma)\frac{d^2N_\gamma}{dE_\gamma dt}dE_\gamma \tag{44}$$

where $A(E_\gamma)$ is the effective area of the detector, as a function of photon energy E, and r is the distance from the PBH to the detector.

In this paper, we will use the HAWC observatory [13] as a representative VHE gamma-ray observatory to investigate the PBH observational signatures. Fig. 14 shows the detection time profile for a PBH burst at a distance $r = 0.015$ pc, in the HAWC energy range (50 GeV–100 TeV) and for the HAWC effective area published in reference [40]. As discussed later, if the actual local PBH density is equal to the present limit on the local PBH density, HAWC might expect to have a 30% chance of observing such a burst (at 0.015 pc or closer) within its instantaneous field of view during 5 years of data taking.

An interesting feature of the BH signal is that the detection time profile (Fig. 14) rises more rapidly than the source emission time profile (Fig. 12) as the remaining evaporation lifetime $\tau \rightarrow 0$. This occurs because the effective area $A(E_\gamma)$ is largest at high photon energies, $E_\gamma > 10$ TeV, where both direct and fragmentation photon components are important but have different energy dependencies.

The HAWC detection time profiles for various photon energy ranges, analogous to the burst emission time profiles shown in the bottom panel of Fig. 13, are displayed in Fig. 15.

4. PBH burst searches and upper limits

4.1. PBH burst Simple Search (SS) method

The most straightforward way to search for a PBH burst (or any burst) is to define search windows for the data in both time and space (i.e., angular position on the sky), and then to inspect the search windows for excess over the expected (sky and instrument) background; the manner in which search intervals are defined, and threshold levels set, varies. For a given detector, this Simple Search (SS) method can be divided into two categories: the blind untriggered SS and the externally triggered SS. In a blind search, the time and location of the burst is not a priori known, and hence all temporal and spatial windows need to be inspected for an excess over the background. This may incur a large number of trials and correcting for them may reduce the sensitivity of the search. An externally triggered search, on the other hand, will look at a certain time and sky position for a burst once the burst has been detected in another detector. Depending on how accurately the time and location of the externally triggered burst is known, a triggered search can incur typically one or a few trials, significantly less than a blind search.

For both SS categories, we need to estimate the minimum number of expected signal counts, $\mu_\circ$, required for a statistically significant burst detection to be probable. The value $\mu_\circ$ may depend on the duration of the search window and its location in the detector's field. In order to calculate $\mu_\circ$, fluctuations in both the background and the signal need to be considered. First, let n be the number of counts which has a probability of less than $p_0 \sim 2.87 \times 10^{-7}$ (corresponding to 5σ) of occurring under the background-only hypothesis, after correcting for N_t trials. If the

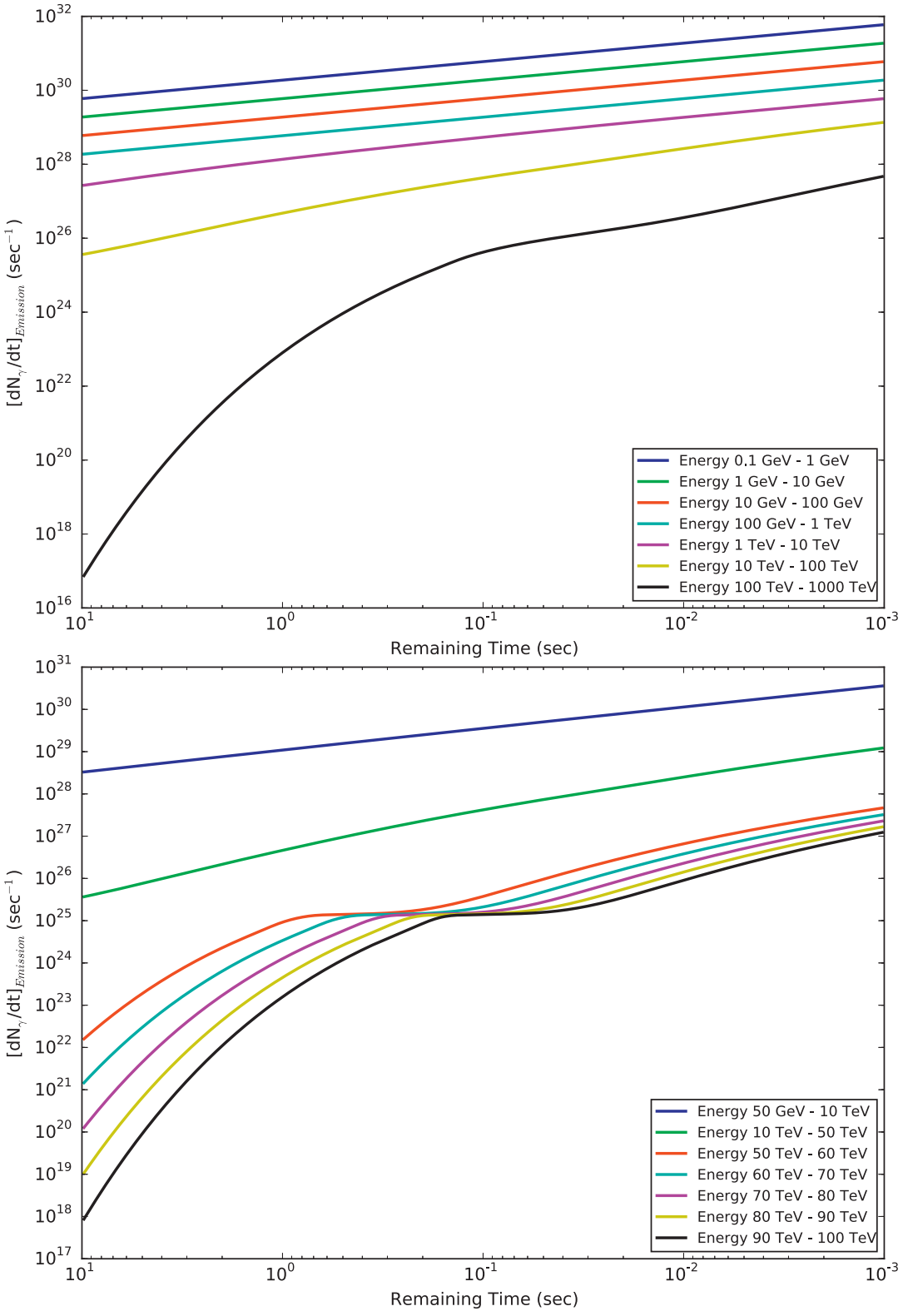

Fig. 13. Top panel shows the BH burst source emission time profile, the emission rate integrated over energy, for various integrated energy ranges. Here the shape of the emission time profile is the same for energy bands less than $\sim$ 10 TeV but is starting to become energy-dependent above $\sim$ 10 TeV. Bottom panel shows the BH burst source emission time profile for a number of energy bands above 10 TeV. Here the energy dependence of the burst profile for higher energy bands can be clearly seen with an inflection region around $\tau \sim 0.1$ s.

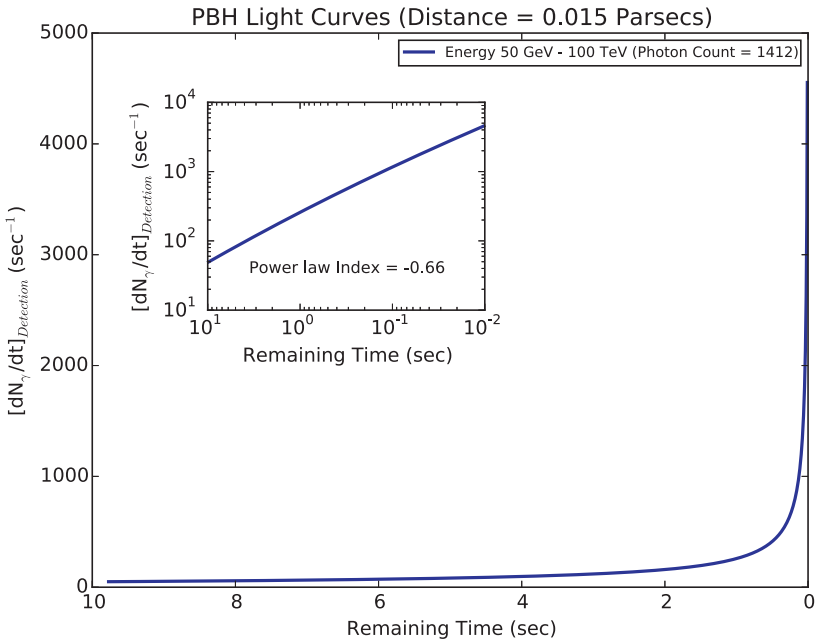

Fig. 14. Simulated PBH burst light curve observed by HAWC (at a distance of 0.015 pc) obtained by convolving with the HAWC effective area published in Ref [40]. This shape is well described by a power law with an index of ~ -0.7.

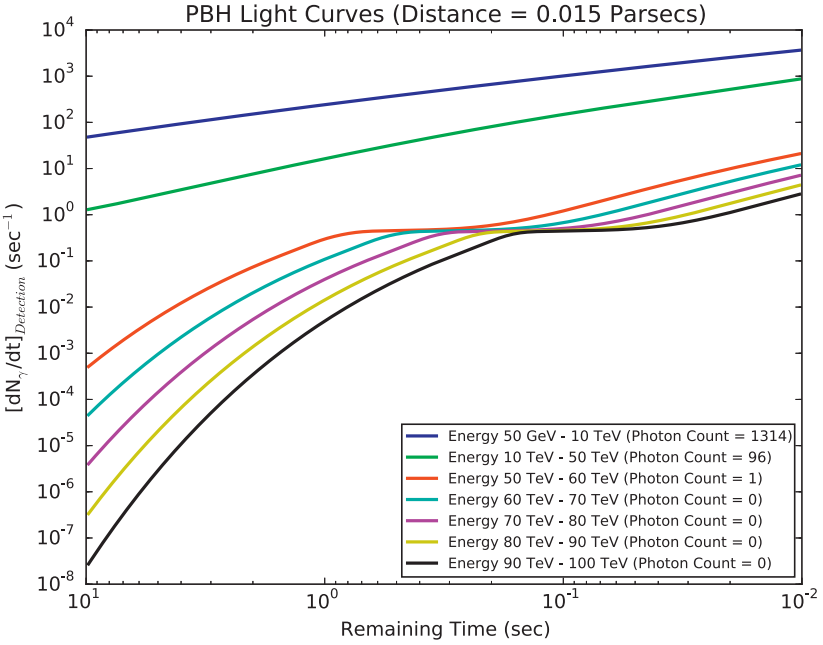

Fig. 15. Simulated detection time profiles of a PBH burst at a distance of 0.015 pc observed by HAWC in multiple energy bands. Photon numbers detected in each energy band are shown in the legend.

detector counts follow a Poisson distribution and B is the mean number of background counts expected over the search window Δt, then n is found from

$$p_c = p_o/N_t = P(\geq n|B). \tag{45}$$

where p_c is the required p-value after correction for N_t trials. The notation $P(\geq n|B)$ denotes the Poisson probability of getting n or more counts when the Poisson mean is B. To estimate $\mu_\circ$, we also need to consider the fact that the signal will fluctuate around some mean. Thus, we need to find the mean value of the signal that together with the background will give the desired n counts in the detector X% of the time. The signal mean is then our $\mu_\circ$ value. In typical searches, X% is taken to be 50%; that is, $\mu_\circ$ is defined as the signal strength needed to give a 5σ detection 50% of the time. Hence, for the SS method, we can estimate $\mu_\circ$ from the equation

$$P(\geq n|(B+\mu_\circ)) = 0.5. \tag{46}$$

Note that with these definitions, $\mu_\circ \approx n - B$ is reasonable approximation. Fig. 16 shows the mean signal counts, $\mu_\circ$, for a 5σ detection 50% of the time for a single trial as a function of background counts, based on the PBH SS method and a Poisson count distribution. The $\mu_\circ$ values derived for a Gaussian distribution are also shown.

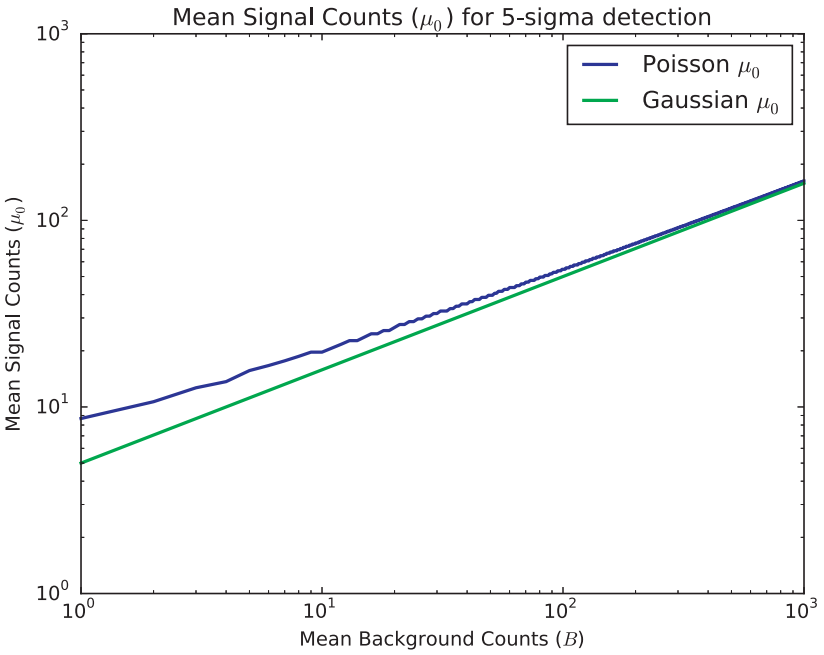

Fig. 16. Number of signal counts needed ($\mu_\circ$) for a 5σ detection 50% of the time for a single trial as a function of the background counts using the PBH Simple Search (SS) method. The $\mu_\circ$ values are shown for a Poisson count distribution (upper blue line) and a Gaussian distribution (lower green line). (For interpretation of the references to colour in this figure legend, the reader is referred to the web version of this article.)

4.2. Binned Maximum Likelihood Search (BMLS) method

The Simple Search (SS) methods of Section 4.1 use all photons detected in the search window irrespective of their energy or time profile. Thus, a SS does not make use of the time profile (the light curve dN_γ/dt) or the energy profile (dN_γ/dE) of the PBH burst which we derived in Section 2. Does utilizing the time profile of the final seconds of the burst, we calculated in Section 3.5, improve search sensitivity? To address this question, we investigate the Binned Maximum Likelihood Search (BMLS) method using a simple Monte Carlo simulation.[9]

Consider a search window of duration Δt. Each search window has an expected background mean (B), and possibly signal mean (S). The background counts are expected to be distributed over Δt with uniform probability while the PBH signal counts are expected to be distributed according to Fig. 14. In the BMLS method, we take advantage of the PBH burst time profile by dividing each search window into k bins of time. If there is a PBH burst in a given window then we expect the signal to be distributed in these k according to Fig. 14. For the purposes of comparison with the SS method, we will imagine that for both the SS and BMLS the search window Δt ends at the expiration of the PBH burst, giving each search the best possible alignment of the search window. Thus, for a given search window, we can write the log of the likelihood ratio of the signal-plus-background hypothesis to the background-only hypothesis as

$$\lambda = \sum_{i=1}^{k} \ln \frac{P(c_i|(s_i+b_i))}{P(c_i|b_i)} \tag{47}$$

where c_i is the observed number of counts in each bin, s_i and b_i are the expected (mean) number of signal and background counts respectively in each bin ($S = \sum_{i=1}^{k} s_i$ and $B = \sum_{i=1}^{k} b_i$), and $P(c|q)$ is the Poisson probability of obtaining c counts when q counts are expected.

Proceeding further, we have

$$\lambda = \sum_{i=1}^{k} \left(\ln \frac{(s_i+b_i)^{c_i} e^{-(s_i+b_i)}}{c_i!} - \ln \frac{b_i^{c_i} e^{-b_i}}{c_i!} \right)$$

which simplifies to

$$\lambda = \sum_{i=1}^{k} c_i \ln\left(\frac{s_i+b_i}{b_i}\right) - \sum_{i=1}^{k} s_i = \sum_{i=1}^{k} c_i \ln\left(1+\frac{s_i}{b_i}\right) - S. \tag{48}$$

If a non-zero signal occurs in a search window, then we estimate its strength as $\hat{S}$, the value of S which maximizes λ, as shown in the top panel of Fig. 17. (In Fig. 17, λ as a function of the expected signal S is shown for a single simulated randomized search window with $\hat{S} = 25$.) The value of λ associated with $\hat{S}$ is denoted by $\hat{\lambda}$. The maximum signal location can be found by partially differentiating Eq. (48) with respect to S,

$$\frac{\partial \lambda}{\partial S} = \sum_{i=1}^{k} \left(\frac{c_i}{s_i+b_i}\right) \frac{\partial s_i}{\partial S} - 1. \tag{49}$$

Setting $s_i = S f_i$ where f_i is the normalized binning of the PBH light curve shown in Fig. 14, we find

$$\frac{\partial \lambda}{\partial S} = \sum_{i=1}^{k} \left(\frac{c_i f_i}{S f_i + b_i}\right) - 1 \equiv Q(S) - 1. \tag{50}$$

For λ to be a maximum at $S = \hat{S}$, we require $\partial\lambda/\partial S = 0$ at $S = \hat{S}$ and so

$$Q(\hat{S}) = \sum_{i=1}^{k} \left(\frac{c_i f_i}{\hat{S} f_i + b_i}\right) = 1. \tag{51}$$

Because Eq. (51) is not analytically solvable, we numerically evaluate $Q(S)$ and $Q(\hat{S})$, as shown in the bottom panel of Fig. 17. Noting $Q(S)$ is monotonically decreasing, we employed an efficient binary search algorithm to find $\hat{S}$.

[9] We also note that the energy profile of the burst may improve the search sensitivity. For example, the background of the detector may vary with the energy, and the detector may be more sensitive in certain energy ranges. However, we defer investigation of energy profile considerations to a separate paper.

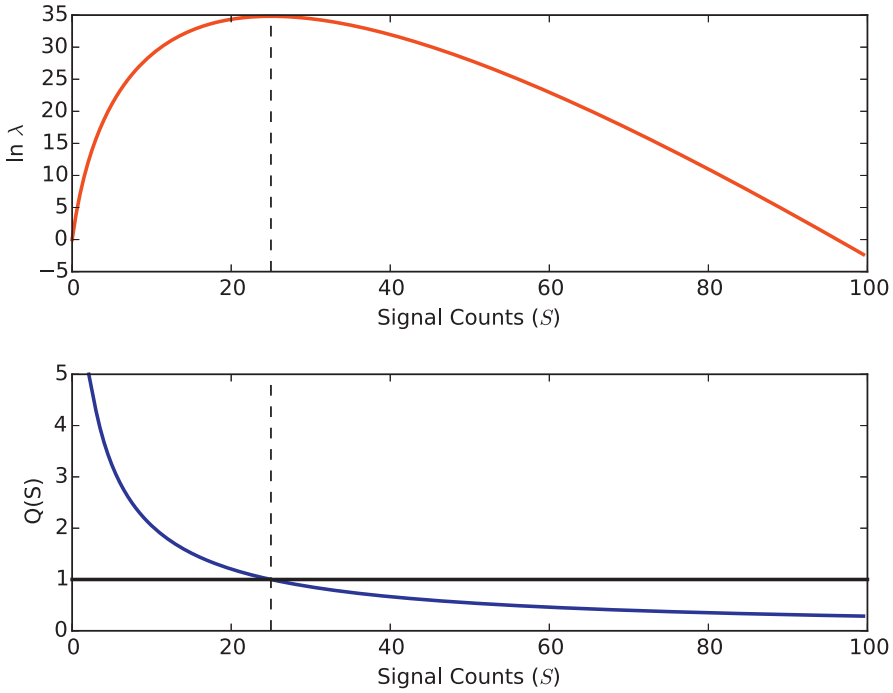

Fig. 17. Log likelihood ratio (upper panel) and $Q(S)$ (lower panel) as a function of S for a simulated Binned Maximum Likelihood Search (BMLS) bin with $\hat{S} = 25$. The log likelihood ratio is a maximum, i.e., $S = \hat{S}$, where the function $Q(S) = 1$.

In order to find μ_0, the mean number of expected signal counts necessary for a probable statistically significant detection using the BMLS method, we need two levels of simulation. First, we perform a background-only simulation to obtain the distribution of $\hat{\lambda}$ for background only, and determine λ_c, the value of $\hat{\lambda}$ corresponding to p_c, the p-value for 5σ significance, as for the SS method. We then perform a second set of simulations, varying the expected signal mean until the BMLS finds $\hat{\lambda} > \lambda_c$ half the time, i.e., with a probability of 0.5. For the background-only simulation, we use $\hat{\lambda}$ as a test statistic instead of the signal strength $\hat{S}$ because, although $\hat{\lambda}$ and $\hat{S}$ are correlated, the log likelihood ratio $\hat{\lambda}$ more explicitly answers the question, "is this search more signal-like than background-only-like?".

For our BMLS, we chose k time bins of equal duration. In the background-only simulation, we generate events in each bin by setting $c_i \sim Pois(k^{-1}B)$, where k is the number of bins, B is the expected background mean, and the notation $c_i \sim Pois(\beta)$ denotes that c_i is a random number generated from a Poisson distribution with mean β. For each iteration, we find and record $\hat{\lambda}$. The procedure is repeated a large number of times to find λ_c. This defines our criterion for a detection.

For the signal-plus-background simulation, we run simulations with signal mean S and vary S until the search finds $\hat{\lambda} > \lambda_c$ 50% of the time. The number of events in each bin is generated according to

$$c_i^{sim} \sim Pois\left(Sf_i + \frac{B}{k}\right) \tag{52}$$

The signal-plus-background simulation process is illustrated in Fig. 18. A good starting estimate for S is the value corresponding (on average) to λ_c, which itself can be estimated by recording the $\hat{S}$ values during the background-only simulation.

The results of the BMLS simulation compared with the SS for PBH bursts are shown in Fig. 19. For a value of B corresponding roughly to the conditions of the HAWC 10 s expected limit in reference [13], the BMLS method would produce an upper limit approximately a factor of 1.3 better than the SS method, using the detector-related methods which we describe below in Section 4.3 [13].

We have also investigated the Unbinned Maximum Likelihood Search method using the complete unbinned time profile ("chirp") of the PBH signal. The unbinned search, however, results in little gain compared to a $k = 10$ bin search under the conditions of the present study, namely moderate background events (less than 50) in the search window, and the simplifying assumption that we externally know the burst time. Further studies are under way and will be reported in a separate paper.

4.3. PBH upper limit estimation

In the case of a null detection (i.e., if no PBH bursts are observed), we can derive an upper limit on the local PBH burst rate density, i.e., the number of PBH bursts per unit volume per unit time in the local solar neighborhood. To calculate the upper limit, the PBH detectable volume for a given detector is needed. The expected number of photons received by a detector at or near Earth from a PBH burst during the last τ seconds of its evaporation lifetime at a non-cosmological distance r and at detector angle θ is

$$\mu(r, \theta, \tau) = \frac{(1-h)}{4\pi r^2} \int_{E_1}^{E_2} \frac{dN_\gamma(\tau)}{dE_\gamma} A(E_\gamma, \theta)\, dE_\gamma. \tag{53}$$

In this expression, $dN_\gamma(\tau)/dE_\gamma$ is the PBH photon emission energy spectrum integrated from a remaining burst lifetime $\tau' = \tau$ to $\tau' = 0$. We implicitly assume that the search window Δt has been chosen to end at or near $\tau' = 0$. The function $dN_\gamma(\tau)/dE_\gamma$ can be approximated using Eq. (42). The energies E_1 and E_2 are the lower and upper bounds, respectively, of the energy range of the detector, h is the dead time fraction of the detector, and $A(E_\gamma, \theta)$ is the effective area of the detector as a function of E_γ and θ. The detector angle θ can be the zenith angle for ground-based detectors

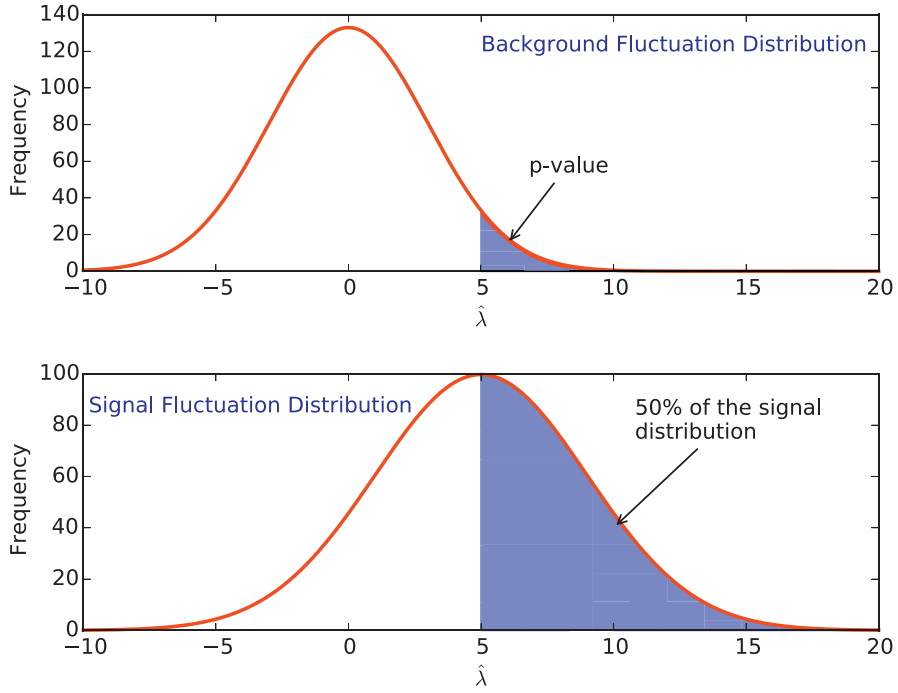

Fig. 18. The number of mean signal counts (μ_0) needed for a 5σ detection 50% of the time is found by first simulating many background-only searches. From the resulting distribution of the maximum log likelihood $\hat{\lambda}$ values (upper panel), we find the value required ($\lambda_c = 5$ in this case) for the desired p-value. We then simulate many searches containing both signal and background events. In the bottom panel we show the distribution of the test statistic $\hat{\lambda}$ for the signal-plus-background case which produces $\hat{\lambda} > \lambda_c = 5$ with a probability of 50%. A smaller value of the expected signal μ_0 would give a smaller fraction of searches passing the $\hat{\lambda} > \lambda_c$ criterion.

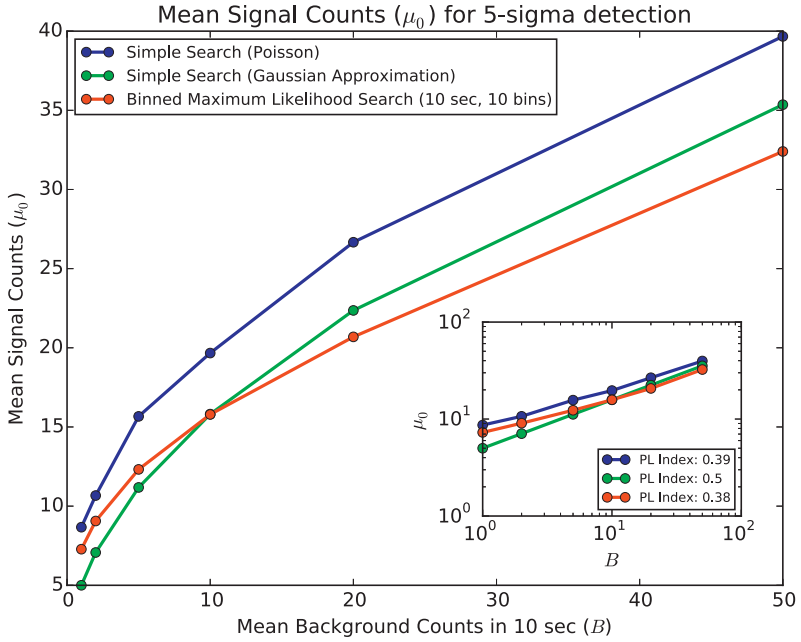

Fig. 19. Comparison of the two PBH burst search methods investigated in this paper: the Simple Search (SS) method and the Binned Maximum Likelihood Search (BMLS) method. The legend identifies the curves at large B in top to bottom order (blue, red, green). The insert shows the power law (PL) indices of the dependence of μ_0 on B. Both search methods have similar power law dependencies. (For interpretation of the references to colour in this figure legend, the reader is referred to the web version of this article.)

or the bore sight angle[10] for space-based detectors. The function $A(E_\gamma, \theta)$ is typically obtained from a simulation of the detector.

In Sections 4.1 and 4.2, we estimated the minimum number of expected signal counts needed for a detection, $\mu_\circ$. By setting μ_0 equal to $\mu(r, \theta, \tau)$, the expected number of counts from a PBH burst at a distance r from Earth, we can solve Eq. (53) to find the maximum distance from which a given detector can detect a PBH burst (with a detection probability of 50%),

$$r_{\max}(\theta, \tau) = \sqrt{\frac{(1-f)}{4\pi\,\mu_\circ} \int_{E_1}^{E_2} \frac{dN(\tau)}{dE_\gamma} A(E_\gamma, \theta)\, dE_\gamma}. \tag{54}$$

[10] Bore sight angle is the angle between the pointing direction of the spacecraft and a source in its field-of-view.

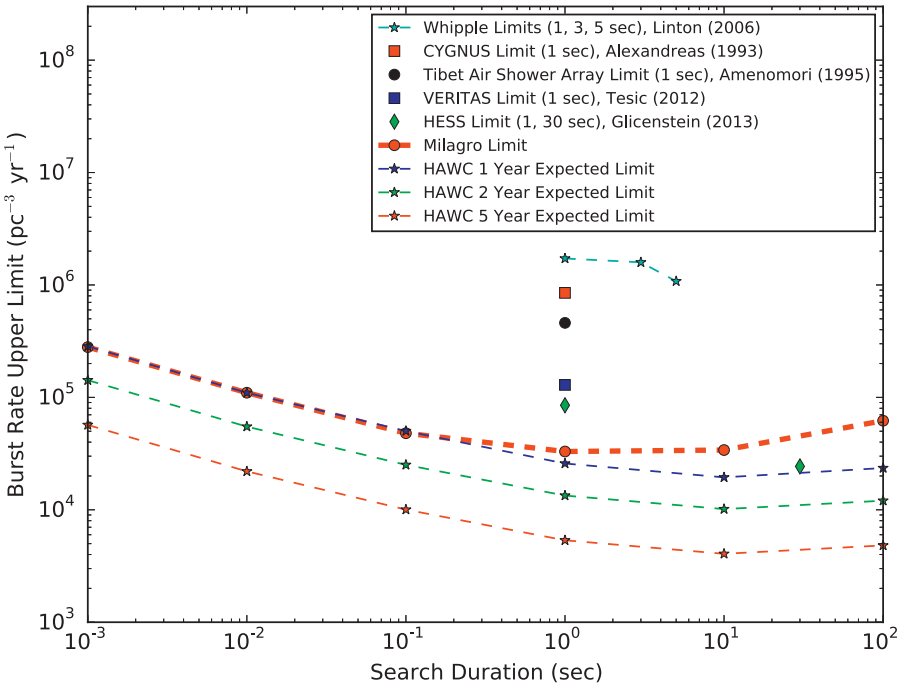

Fig. 20. Published PBH burst rate density 99% CL upper limits and sensitivities for various experiments [7–13]. The upper limits and sensitivities shown are derived using the Standard Emission Model description for the PBH emission spectra.

The total PBH detectable volume of the detector is then

$$V(\tau) = \sum_{\theta} V(\theta,\tau) = \frac{4}{3}\pi \sum_{\theta} r^3_{\max}(\theta,\tau)\frac{\mathrm{FOV}_{\mathrm{eff}}(\theta)}{4\pi}, \quad (55)$$

where $\mathrm{FOV}_{\mathrm{eff}}(\theta)$ is the effective field-of-view associated with the detector angle θ and the summation is over the bands of θ of the detector [13].

If zero PBH bursts are observed, then the Y% confidence level upper limit (UL_Y) on the rate density of PBH bursts, assuming that PBHs are uniformly distributed in the solar neighborhood, can be estimated as

$$UL_Y = \frac{m}{VD}. \quad (56)$$

Here V is the effective PBH detectable volume, D is the total search duration (typically in years) and m is the upper limit at the Y% confidence level on the expected number of PBH events given that zero bursts are observed. Note that for Poisson fluctuations, $P(0|m) = m^0 e^{-m}/0! = 1 - Y$ implies that $m = \ln(1/(1-Y))$. For $Y = 99\%$, $m = \ln 100 \approx 4.6$ and hence the upper limit on the PBH burst rate density in the case of null detection will be

$$UL_{99} = \frac{4.6}{VD}. \quad (57)$$

Fig. 20 shows published PBH burst rate density 99% CL upper limits and sensitivities as a function of the search window, Δt, for various experiments. The PBH rate density limits calculated for Milagro and projected for HAWC are strictest around search window durations of 1 s and 10 s respectively. These optimum burst search intervals reflect the characteristics of the observatory and dependence of the background.

Let us understand the general features of Fig. 20. From Eqs. (54) to (57), we can see that UL, the upper limit on the local PBH rate density, scales as

$$UL \sim (\mu_0(\Delta t)/N_\gamma(\tau))^{3/2} \quad (58)$$

where μ_0 is the sensitivity for a given search window Δt, and $N_\gamma(\tau)$ is the number of observable photons produced by the source over its remaining burst lifetime τ. Better sensitivity corresponds to smaller μ_0, the number of signal photons required for detection of a signal, and a stricter PBH limit. For a source at a given distance (e.g., the one at the outer edge of the volume considered), $N_\gamma(\tau)$ decreases when the search window is shorter, and produces a weaker PBH limit. Shorter search windows incur less background events but also see fewer source photons. In this case, μ_0 is dominated by statistical fluctuations, in particular those associated with the detector background rate, i.e., from Fig. 19, $\mu_0 \propto B^{0.38} \propto (\Delta t)^{0.38}$; and $N_\gamma(\tau)$ is determined by the integral of the PBH time profile, slightly modified by the energy-dependent effective area of the detector, i.e., from Fig. 14, $N_\gamma(\tau) \propto \int_0^\tau t^{-0.66} \propto (\Delta t)^{0.34}$. These dependencies of μ_0 and $N_\gamma(\tau)$ are both power laws and, despite their very different physical origins, nearly cancel. Secondary effects such as the larger number of trials incurred for shorter search windows ($N_t \propto 1/\Delta t$), and the ability to optimize background rates for larger Δt (for which the detection efficiency is higher) give the Δt-dependence seen in Fig. 20.

Thus, in summary, the shape of the PBH limit curves will be similar but will need to be evaluated for each gamma-ray detector. The improvements suggested in this paper, of including the energy and time dependence of the PBH signal, will typically decrease the required μ_0. We anticipate that the PBH burst rate density limit may particularly improve at longer search windows Δt as a result.

4.4. Differentiating the PBH burst from other GRBs

Another important question regarding PBH burst detection is how to differentiate a PBH burst from commonly detected GRBs of known cosmological origin. In particular, some short GRBs of duration less than 2 s have light curves which are very similar to the BH burst emission time profile shown in Fig. 12 [41].

Multi-wavelength observations are very important in differentiating PBH bursts from other known GRB source types. Almost all GRBs have low-energy or VHE afterglows of recognizable shape which follow the main gamma-ray burst. In the case of a PBH burst, no further signal is expected once the BH gamma-ray burst

Table 2
A summary of potential observational differences between standard cosmological GRBs and PBH bursts.

Gamma-ray bursts (GRB)	PBH bursts
Detected at cosmological distances	Unlikely to be detected outside our Galaxy
Time duration can range from fraction of second to few hours	Time duration is most likely less than few seconds
May have multi-peak time profiles	Single-peak time profile
Typically a single peak shows Fast Rise Exponential Decay (FRED) time profile	Power-law Rise Fast Fall (PRFF) time profile expected
X-ray, optical, radio afterglows are expected	No multi-wavelength afterglow is expected
Most GRBs show hard-to-soft evolution	Soft-to-hard evolution is expected from PBH bursts
Cosmic-rays are not expected to arrive from GRBs	Cosmic-ray bursts are expected from nearby PBH bursts
Gravitational wave signal is expected	No gravitational wave signal is expected
Neutrino burst may be seen	Simultaneous neutrino burst may be seen from nearby PBH
TeV radiation may be cut off either at the source or by the intergalactic medium	TeV signal is expected during the last seconds of the burst

has expired, with the possible exception of a signal generated by interaction of the charged emitted particles with the ambient medium if the PBH is embedded in a sufficiently dense or turbulent ambient plasma or magnetic field [3]. The prompt burst time profile in various energy bands may also be used to distinguish a PBH origin. Most GRBs show multi-peak structure with individual pulses exhibiting a Fast Rise Exponential Decay (FRED) shape. The light curve from a BH burst occurring in free space is not expected to exhibit multi-peak structure at detector energies: for an isolated PBH a single short peak described by Power-law Rise Fast Fall (PRFF) as shown in Fig. 12 is expected. In addition, most GRB light curves show hard-to-soft energy evolution while soft-to-hard energy evolution is expected with PBH burst light curves.

Moreover, with respect to TeV gamma-ray observations, the extension of cosmological GRB spectra into TeV energies is uncertain because of the attenuation of gamma-rays from distant GRBs by pair-production off the intergalactic medium (IGM) and the possibility of a cutoff in the GRB source spectrum [42,43]. In contrast, local PBH bursts have a spectrum which extends well above 1 TeV during the latter parts of the BH burst (for intervals as long as 100 s). Current instruments are sensitive to local PBH bursts ($<$ 1 pc) [13], where the ISM is not expected to significantly attenuate TeV photons. Thus, detection in TeV observatories, together with the other characteristics expected for a BH burst, will lead to a potentially unique identification of the PBH signal.

In addition, GRBs due to PBH bursts are not expected to be accompanied by gravitational wave radiation. GRBs from other sources may be accompanied by gravitational waves (GW) and for short GRBs, a GW signature would confirm a compact star merger origin (which is the leading model for short GRBs). Moreover, we expect the emission of a neutrino burst and cosmic-ray ($e^{\pm}$, p, $\bar{p}$ and possibly n) burst of similar time profiles to accompany the gamma-ray radiation in the event of a BH burst. These neutrino and cosmic-ray bursts should be emitted simultaneously by the BH with the gamma-ray burst. Thus far the reason that we have not detected neutrinos from standard GRBs may be due to their great distances. However, any PBH burst candidate that we detect with the current instruments should be very local, and so VHE neutrino and/or cosmic-ray telescopes may possibly detect the accompanying neutrino or cosmic-ray bursts from a PBH [18,19,44]. Table 2 summarizes the observational differences between standard cosmological GRBs and PBH bursts.

5. BH bursts with high-energy physics beyond the Standard Model

Our analysis in Section 4 is based on the Standard Model of high-energy physics, in which the Hawking-radiated fundamental quanta are limited to those whose existence has been confirmed in high-energy experiments: the photon, neutrinos, charged leptons, quarks, gluons, W and Z bosons, and the 125 GeV Higgs boson. There is strong evidence, however, that the Standard Model is incomplete. For example, observations of neutrino oscillations cannot be explained within the Standard Model and raise the question: are the neutrinos Dirac fermions (with four degrees of freedom for each of the three neutrino flavors) or Majorana fermions (with two degrees of freedom for each of the three neutrino flavors)? To date, only six neutrino degrees of freedom have been observed in detectors and so we assumed in Sections 2–4 that the neutrinos are Majorana fermions.

Other additional fundamental particle species may arise in Beyond the Standard Model (BSM) theories. For example, supersymmetry (SUSY) would imply the existence of SUSY partners for all the known Standard Model quanta: each $s = 1/2$ fundamental Standard Model field would have an $s = 0$ superpartner field and each $s = 1$ fundamental Standard Model field would have an $s = 1/2$ superpartner field. Examples of other BSM theories with additional degrees of freedom include extra dimension theories which imply massive Kaluza–Klein excitations of known fields; shadow sector theories; and technicolor [45,46]. In such models, the function $\alpha(M_{BH})$ would increase at each new rest mass threshold, and thus the asymptotic rate of BH evaporation would be faster than the SEM rate and the remaining BH lifetime would be shorter. The observable spectra may be further modified, depending on the degree to which the new particle species couple to ordinary matter and their decay characteristics. Hence it is possible that BSM physics may modify our predictions for the observation of the final stages of PBH evaporation. If new degrees of freedom only manifest well above 100 TeV, however, there will be little overall change to our analysis of Sections 2–4.

We note too that in this paper we are analyzing 4D black holes or black holes that approximate 4D BHs. Higher-dimensional theories with $(n+4)$-dimensional gravity would have a lower Planck mass. At very high T_{BH} in such extra dimension theories, the equations relating black hole mass, temperature and remaining lifetime and the emission spectra are significantly different to those of 4D BHs once the BH Schwarzschild radius becomes smaller than that of the extra dimensions. For recent reviews on accelerator limits on $(n+4)$-dimensional black holes see Refs. [47–49].

In the following subsections, we address in greater detail the modifications to the 4D BH spectra that would arise from Dirac neutrinos or SUSY.

5.1. Dirac neutrinos

If neutrinos are Dirac fermions, the value of α must be modified. We can estimate the effect at high T_{BH} as follows. The total Hawking-radiated power determines the rate at which the BH mass decreases. The function $\alpha(M_{BH})$, which is defined by Eq. (11), accounts for the radiation of all relevant fundamental particle species by an M_{BH} black hole. For the detection of the final gamma-ray burst from a BH, we are interested in remaining evaporation lifetimes in the range $\tau < 100$ s. Including the six extra degrees of freedom of Dirac neutrinos would increase the asymptotic

($\tau < 100$ s) value of $\alpha(M_{BH})$, which we took in Sections 2–4 to be α_{SM}, by 12% with little change to our analysis.

If the extra Dirac neutrino degrees of freedom are light, $\alpha(M_{BH})$ would be increased at large M_{BH} by a greater percentage. In particular, if the rest masses of the extra Dirac neutrino modes are lighter than about 100 MeV, the initial mass of a PBH whose lifetime equals the present age of the universe would be larger than the SEM value of 5×10^{11} kg by up to 15%.

5.2. Black Hole emission with supersymmetry

To examine the question, would the contributions from new BSM particles be discernable at a VHE gamma-ray observatory if the observatory observes a PBH burst with a duration of $\tau \sim 100$ s, we now consider a supersymmetric (SUSY) state to which HAWC might be sensitive. We focus on squarks (the $s = 0$ superpartners of quarks) because they represent a large number of degrees of freedom at a single threshold (due mainly to their color degree of freedom), they decay into quarks which in turn decay into $\pi^0 \rightarrow \gamma\gamma$ resulting in observable TeV photons, and they are $s = 0$ scalars with more intense Hawking flux and power than higher spin states. The general statement, that the TeV photon emission rate increases at the rest mass threshold corresponding to the new TeV particle mode, applies to whatever BSM theory is the origin of the new particle mode and hence their consequences, while not identical, would resemble, or be weaker than, the squark radiation case. The total Hawking flux and power will depend on the number of degrees of freedom and spin of the new particle mode. For example, extra dimensional theories as a class may produce numerous new states, some of which are colored. The effects of colored states would likely resemble those of squarks, but have a weaker influence on the final photon spectra unless the states were also $s = 0$ scalars. Non-colored states such as gauge particles or lepton-like particles would be expected to have less effect on the TeV photon spectra because of their fewer degrees of freedom, higher spin, and/or less frequent photon decays.

In SUSY models, such as the minimal supersymmetric standard model (MSSM), there are many new fundamental superpartner fields. Let us consider the case of a superpartner that is a squark of mass m_{sq}. Once $kT_{BH} \gtrsim T_{sq} \equiv m_{sq}c^2/x_{p,s=0}$, this squark species will appear in the Hawking radiation in significant numbers. The squark will then decay into a quark and other particles, with the quark then fragmenting and producing photons as described in Section 2.

Let τ_{sq} be the remaining burst lifetime when the BH temperature reaches T_{sq}. If τ_{sq} is much larger than 100 s—the time window of the search—then a BH burst which includes squark emission cannot be distinguished from an SEM BH burst because the distance to the observed BH is undetermined: a BSM BH burst with squark radiation would produce approximately the same signal in the detector as a closer SEM BH burst.

On the other hand, if $\tau_{sq} < 100$ s, the observatory may witness the photon rate increasing due to squark radiation as the remaining BH evaporation lifetime becomes less than τ_{sq}, provided the burst flux in the detector is large enough.

In many SUSY models, such as those tested at the LHC, the rest masses of the superpartners are assumed to be of the order 500 GeV to 1 TeV, which correspond to threshold times τ_{sq} much greater than 100 s. (If the squark mass is of order 5 TeV, then $kT_{sq} = 1.9$ TeV and the threshold time $\tau_{sq} \lesssim 70$ s (from Eq. (22)) would occur during the time window of the PBH search.) The value of the remaining burst lifetime τ_{sq}, though, depends on $\alpha(M_{BH})$. If we assume that the evaporation process is dominated by SEM particles until T_{BH} reaches T_{sq}, then

$$\alpha(M_{BH}) = \alpha_{SM} \quad \text{for } 10^8 \text{ kg} \gtrsim M_{BH} > M_{BH,sq} \tag{59}$$

where $M_{BH,\,sq}$ is the BH mass threshold corresponding to T_{sq}. (For a 5 TeV squark, $M_{BH,sq} = \hbar c^3/(8\pi GkT_{sq}) = 5.5 \times 10^6$ kg.) For $M_{BH} < M_{BH,\,sq}$, $\alpha(M_{BH})$ increases by the contribution due to the squark emission, i.e.,

$$\alpha(M_{BH}) = \alpha_{SM} + \alpha_{sq} \quad \text{for} M < M_{BH,sq}. \tag{60}$$

Here the contribution from the squark degrees of freedom is

$$\alpha_{sq} = 1.7 \times 10^{17} \text{ kg}^3 \text{ s}^{-1} \tag{61}$$

noting that the number of degrees of freedom for a squark with left-handed and right-handed states of the same mass is 12 (particle, antiparticle, handedness, and 3 color modes) and $\Phi_{s=0} = 6.89$ for each squark degree of freedom.

Fig. 21 shows the masses of an SEM BH and the BSM BH as a function of the remaining lifetime τ of the SEM black hole, assuming for alignment purposes that both BHs had the same mass when $\tau \gg \tau_{sq}$. In this example, the threshold time for emission of the squark is $\tau_{sq} = 70$ s and the BSM BH burst expires at $\tau_F = 12$ s. The value of $\alpha(M_{BH})$ is given by Eqs. (59) and (60).

5.3. Statistical estimate of detection sensitivity to squark emission

Let us make a rough estimate of the observational sensitivity to the SUSY squark threshold. As shown in Fig. 20, a likely search interval for the HAWC observatory lies within the range of 10–100 s. The rest mass of a squark which would fall within this search window range is then given by

$$m_{sq}c^2 \simeq 7.8x_{p,s=0}\left(\frac{1\text{ s}}{\tau_{sq}}\right)^{1/3} \text{TeV} \tag{62}$$

(see Eq. (21)), i.e., $m_{sq}c^2 \simeq 5$–10 TeV for $10\,\text{s} \lesssim \tau_{sq} \lesssim 100\,\text{s}$. Because the value of α will increase due to the Hawking radiation of the SUSY states, the actual remaining time will be somewhat shorter, and the squark mass range somewhat higher than this estimate.

The observational signature of a SUSY superpartner threshold being passed by the BH would be an enhanced photon rate at shorter remaining burst lifetimes (i.e., when $T_{BH} \gtrsim T_{sq}$), compared to the rate at earlier times. To estimate the extent to which discerning such a rate increase is feasible, we consider the following conservative simplified model. A squark is expected to decay into a quark and the Lightest SUSY Particle, typically a neutralino. If the neutralino mass is not a large fraction of the initial squark mass, then the quark should generate a photon spectrum similar to that generated by a directly Hawking-radiated quark of the same initial energy as the squark. To count the number of degrees of freedom of the initial squark, we conservatively assume a squark of a single handedness and hence only six degrees of freedom (particle, antiparticle and three colors modes), rather than the 12 squarks degrees of freedom assumed in Eq. (60). Recalling from Section 2.1 that $\Psi_{s=0} = 2.8\Psi_{s=1/2}$, we expect that each squark degree of freedom is Hawking-radiated 2.8 more often than each quark degree of freedom when $T_{BH} \gtrsim T_{sq}$. Thus, noting that there are 72 total degrees of freedom for the $s = 1/2$ SEM quarks, the squark emission enhances the overall BH photon rate by a factor of about $6 \times 2.8 \div 72 \simeq 23\%$. Fig. 22 compares the photon emission rate for the SEM BH and the BSM BH with $\tau_{sq} = 70$ s and $\tau_F = 12$ as a function of the remaining lifetime of the SEM BH, assuming that both BHs had the same mass when $\tau \gg \tau_{sq}$ and the squark emission enhances the observable photon rate by 23%.

In the same spirit, let us use a simple analysis to estimate the detectability of this photon rate increase. Let us assume that the power law of the BH photon burst emission time profile shown in Fig. 12 is little changed after the SUSY superpartner threshold is reached, i.e., that the increase in α due to the SUSY states at τ_{sq} is negligible. We compare the number of photons in the final 10 s of

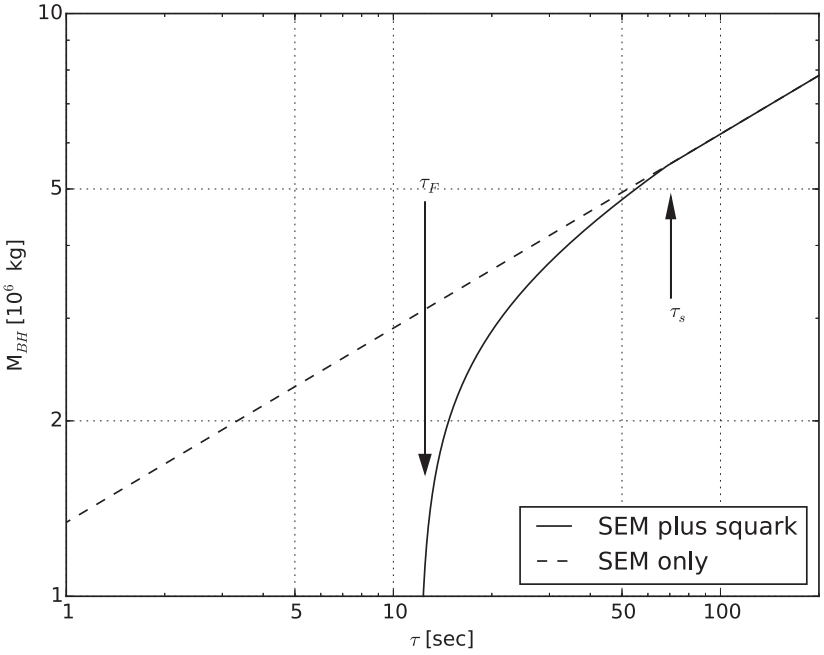

Fig. 21. Black hole mass of an SEM BH and a BSM (SUSY) BH as a function of the remaining lifetime of the SEM BH. The time threshold for squark emission by the BSM BH is $\tau_{sq} = 70$ s; the completion of the BSM BH burst occurs at $\tau_F = 12$ s. Solid curve: the BSM black hole with squark radiation. Dashed curve: the SEM black hole.

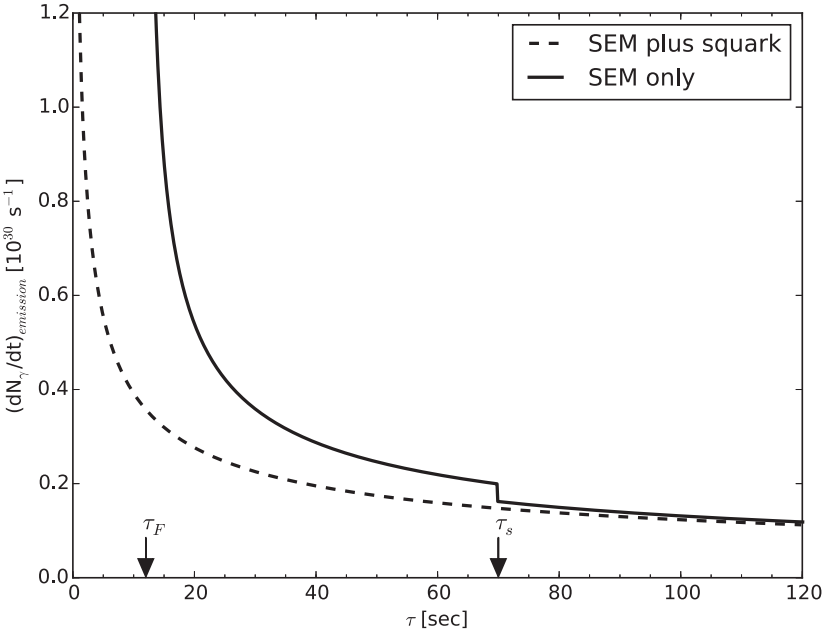

Fig. 22. Black hole photon emission rate of an SEM BH and a BSM (SUSY) BH as a function of the remaining lifetime of the SEM BH. The time threshold for squark emission by the BSM BH is $\tau_{sq} = 70$ s; the completion of the BSM BH burst occurs at $\tau_F = 12$ s; and the squark emission is conservatively estimated to enhance the observable photon rate by 23%, as discussed in Section 5.3. Solid curve: the BSM black hole with squark radiation. Dashed curve: the SEM black hole.

the BH burst, with the number of photons seen in an earlier longer interval, say between 80 and 200 s prior to the end of the burst. Assuming the photon rate is enhanced by ∼20% as estimated above for a squark threshold in the range $10\,\text{s} \lesssim \tau_{sq} \lesssim 80\,\text{s}$, and applying the power law of Fig. 12, the ratio of the number of photons in the 80-200 s interval is 0.97 times that in the 0-10 s interval for the SEM BH, while it is 0.79 times that in the 0-10 s interval for the SUSY BH. Taking the case considered in Fig. 14 of a nearby PBH burst at 0.015 pc whose final 10 s would produce a photon count of ∼1400 photons at the HAWC observatory, we find, considering Poisson fluctuations only in the number of signal photons and ignoring background fluctuations, that the SEM BH burst and a BSM BH burst with a squark threshold of $10\,\text{s} \lesssim \tau_{sq} \lesssim 80\,\text{s}$ would be distinguishable with a significance above 4 standard deviations.

Thus it is clear that detection of a nearby PBH burst has an interesting sensitivity to multi-TeV squark states which are currently inaccessible with hadron colliders. Further refinements of these calculations and other SUSY models will be presented in a separate paper.

6. Discussion

Our analysis in Sections 2–4 assumes the SEM of black hole radiation based on the Standard Model of high-energy physics and

the Hawking radiation of fundamental particle species, such as quarks and gluons, as initially asymptotically free particles. If a direct PBH burst search is unsuccessful, the null result will constrain the local density of such PBH burst events but any derived upper limit will depend on the validity of the SEM. Alternative emission theories make different predictions for the PBH photon emission rate and/or spectrum. Here we discuss some issues arising from our SEM-based analysis.

6.1. The pion fragmentation function for quarks and gluons

In this paper, we assumed that all Hawking-radiated quarks and gluons fragment and hadronize into pions, according to the fragmentation function in Eq. (24). Is the pion fragmentation function employed in Section 2 a realistic approximation?

Fragmentation functions have been extracted from accelerator data, e.g. from electron–positron collider experiments. The heuristic model in Eq. (24) agrees qualitatively with the empirical fragmentation functions [32], although the quantitative accuracy is limited. Two aspects of the fragmentation process are absent from the heuristic model. First, the assumption that all flavors of quarks eventually fragment equally and completely into pions is not strictly true. The fragmentation steps will also produce other mesons and baryons. In addition, heavy particles such as the top quark, $W^{\pm}$, Z^0 and H initially decay into lighter quarks rather than directly undergoing hadronic fragmentation into pions; the fragmentation function into pions for these heavy particles will feature fewer pions at high z than for light quarks, and somewhat more pions with $z < 0.3$ or so. Second, QCD fragmentation functions depend to some degree on the energy scale of the process, whereas Eq. (24) is scale-invariant.

An enhanced treatment of fragmentation and hadronization is possible using either more detailed QCD fragmentation functions or Monte Carlo simulations for the fragmentation and hadronization using parton shower codes like Pythia [36] or Herwig [37]. As we noted in Section 3.1, though, the function Eq. (24) implies an average energy of final state photons and a multiplicity of final state photons per initial parton which match the $T_{BH}^{1/2}$ scaling of photon average energy and multiplicity found using a HERWIG-based Monte Carlo simulation for $1\,\mathrm{GeV} \leq T_{BH} \leq 100\,\mathrm{GeV}$ BH emission spectra [17]. We also showed in Section 3.4 that the time-integrated photon spectrum derived using the fragmentation function of Eq. (24) is in good agreement with the parameterization of the time-integrated spectrum derived by fitting the results of the HERWIG-based Monte Carlo BH simulations. Thus the fragmentation function given in Eq. (24) is adequate for deriving a good estimation of the overall instantaneous photon BH emission spectra.

6.2. Photospheres and other models of intrinsic interaction of BH radiation

The SEM assumes that relativistic quarks and gluons emitted as Hawking radiation escape as asymptotically free particles from their creation region close to the BH horizon (i.e., they do not undergo significant interactions with other Hawking-radiated particles over distances at least up to of order 10^{-15} m appropriately Lorentz-transformed), analogous to quark and gluon jet creation in high-energy collisions in accelerator experiments. (See [3] for the details of this analogy.) Over distances of a few Fermi appropriately Lorentz-transformed, the QCD quanta then undergo fragmentation and hadronization, consistent with observations of high energy accelerator collisions.

Some authors, however, have proposed that in the neighborhood of the BH the radiated particles undergo additional interactions. In these scenarios the Hawking radiation after emission self-interacts to form a dense photosphere around the microscopic black hole [50–52]. The emission rate is not modified but the particle energies are degraded to lower energies in the vicinity of the BH, resulting in a photon spectrum which, at high photon energies, would be less than that predicted by the SEM (Fig. 5). Although the limit derived by the 100 MeV emission from a Galactic or cosmological distribution of PBHs would be only slightly modified, the probability of detecting the high energy gamma ray or cosmic rays bursts from individual PBHs is significantly weakened in photosphere models. For example, the Heckler photosphere model predicts that the photon flux above $E_\gamma \simeq 1$ TeV emitted by a $T_{BH} = 1$ TeV black hole over its remaining lifetime is approximately 4 orders of magnitude less than the $E_\gamma \gtrsim 1$ TeV flux predicted by the SEM analysis [51]. In the Heckler model, the high-energy time-integrated photon spectrum decreases as E_γ^{-4}, not as E_γ^{-3} as shown for the SEM case in Fig. 11.

Recent detailed re-analysis of the published photosphere scenarios, however, has strongly argued that the conditions required for the production of intrinsically-induced photospheres are not met around Hawking-radiating black holes [3]. In particular, the Hawking flux emission rate implies that there is insufficient causal connection between the majority of consecutively emitted particles for QED or QCD interactions to occur between them; the quantum conservation laws and available energy per Hawking-radiated particle, together with the suppression of Γ (see Section 2) near rest mass thresholds, prevent the formation of a QCD photosphere as the BH transitions through the QCD confinement scale; and the long formation distance required for the production of any final state created in an interaction prevents an individual particle undergoing multiple interactions close to the BH. Although one should be cognizant that intrinsically-induced photospheres would change the observational characteristics and limits, we expect that the search methods will be primarily based on the SEM for the next generation of PBH searches.

6.3. Modification of BH burst by ambient environment

Although models for intrinsically-produced photospheres do not seem viable, the possibility exists in the SEM that the observable signal may be modified if the PBH is embedded in, for example, a region of ambient dense plasma or a strong magnetic field [3].

Rees has proposed a model [53] in which the high energy electrons and positions emitted in the final BH burst form a relativistically-expanding conducting shell. The conducting shell is then braked by the ambient Galactic magnetic field, generating a strong radio pulse. The original Rees model assumed that these were exclusively electrons and positrons, and the remaining BH mass, were emitted in one instant once the BH temperature reached $T_{BH} \simeq 0.16$ GeV. Re-analyzing the model using the SEM, extrapolating to higher T_{BH} the emission spectra of Ref. [17] which incorporate quark and gluon emission, and taking a typical interstellar magnetic field of strength $B \simeq 5 \times 10^{-6} b$ G where $b = O(1)$, MacGibbon found that the conditions for the generation of an electromagnetic pulse are not met until the BH mass reaches $M_{pulse} \simeq b^{-1/2} (\alpha(M_{pulse})/\alpha_{SM})^{1/2}$ g [54]. The electromagnetic pulse would now be seen at about $E_\gamma \simeq 70 b^{3/2} (\alpha(M_{pulse})/\alpha_{SM})^{-1/2}$ TeV (with a duration $\Delta t \lesssim 10^{-25}$ s much less than the time resolution of any detector) and contain a total energy of $E_{pulse} \simeq 10^{25} b^{-1/2} (\alpha(M_{pulse})/\alpha_{SM})^{-1/2}$ GeV. If the conditions for the pulse are met, there would be $N_\gamma = E_{pulse}/E_\gamma \simeq 10^{23} b^{-2}$ photons emitted in the pulse. For a typical interstellar magnetic field ($b = O(1)$), the pulse would thus be much weaker than the PBH lightcurves of Figs. 12 and 13. Although these estimates should not be regarded as precise, because they involve the extrapolation of the BH emission spectra to energies well above accelerator energies, it can be stated that the electromagnetic pulse generated by a bursting SEM

BH in the Galactic magnetic field would have a wavelength in the gamma-ray range, not radio range as in the original Rees analysis, and occur at a much smaller M_{BH} thus producing a less-detectable signal.

6.4. PBH evaporation events in the Hagedorn model

Some previous studies of BH burst emission have assumed the Hagedorn model, also called the statistical bootstrap model. This particle physics model, which arose before the existence of quarks and gluons was confirmed in terrestrial accelerators, postulates that there is an exponentially rising spectrum of meson resonances once a threshold temperature Λ_{QCD} has been reached.

The Hagedorn PBH model assumes each of the meson resonances is an independent degree of freedom of Hawking radiation. Thus in the Hagedorn model, the function $\alpha(M_{BH})$ exponentially increases in this temperature regime and the PBH luminosity is correspondingly enhanced. The model also assumes that the remaining mass of the BH will be emitted around this temperature producing a stronger final burst that will be confined to lower photon energies ($\lesssim 1$ GeV), in contrast to the SEM burst.

However, with the discovery of quark and gluon jets in accelerator collisions above Λ_{QCD}, the Hagedorn model is no longer a viable description of particle production in such collider events. Moreover, detailed consideration [3] of the particle separation, energies and timescales of Hawking radiation of QCD particles indicates that the asymptotic freedom of QCD which describes jet production at hadron colliders applies to Hawking radiation.[11] Additionally, because the Hawking radiation of a particle correspondingly reduces the BH mass and hence increases the BH temperature, any Hagedorn phase can at most be temporary with the BH transitioning quickly to temperatures above the Hagedorn regime. The form of the absorption factor Γ of Eq. (1) also strongly suppresses the Hawking emission of a species when T_{BH} is close to the rest mass threshold of the species, thus weakening the signal from any temporary Hagedorn regime. Taken together, these considerations strongly argue against the Hagedorn model applying to BH emission or producing an enhanced PBH burst signal at the detector.

6.5. Do very short gamma-ray bursts originate from PBHs?

Studies of very short gamma-ray bursts (VSGRB), with time durations $\lesssim 0.1$ s, tentatively suggest that these events may form a distinct class of GRBs [55,56]. The data used in these studies come from BATSE, Fermi GBM, Swift, KONUS, and other keV/MeV gamma-ray detectors [55,57,58]. Evidence that the VSGRBs are distinctly different from GRBs of longer duration includes the anisotropy on the sky of the distribution of VSGRBs [56] and the hardness of their photon spectra. The VSGRB sky positions may be clustered close to the anti-galactic center region [56], unlike short or long GRBs, possibly indicating that the VSGRBs may have local origin.

These characteristics of VSGRBs have led to speculation that some fraction of these events may be PBH bursts [55,57,58]. The highest photon energies observed in these VSGRBs are less than 10 MeV. The authors in Refs. [55,57,58] compared the observed light curves with the total flux that would be seen from a nearby PBH burst, assuming that the remaining mass of the PBH is converted into photons with energy well below 1 MeV. The authors found reasonable agreement between the shape of the observed and predicted time profiles, but achieved the best matches by assuming that BH emission is enhanced as T_{BH} approaches a phase transition or as conditions for a 'fireball' photosphere set in. We note, however, that the photon energies of these detectors are much lower than the 50 GeV–100 TeV range which we have analyzed in this paper. Furthermore the behavior of the quark and gluon fragmentation and hadronization functions at photon energies well below 100 MeV is uncertain and our results cannot be simply extrapolated to such low photon energies. Although it is possible that the VSGRBs may ultimately be explained by astronomical processes involving compact objects, such as neutron star mergers in the Milky Way galaxy, we intend in a following paper to address the modeling of the BH burst gamma-ray spectra below 1 GeV using the SEM, motivated by the VSGRB observations and proposals for future telescopes in these lower wavelengths. In any case, PBH searches at TeV-scale observatories should be based on the SEM at $T_{\rm BH} \gg 100$ MeV.

[11] The analysis of Ref. [3] also shows that the conditions for the production of quark-gluon plasma are not met around the black hole.

7. Summary and conclusions

In this paper, we have reviewed and analyzed the theoretical framework of the standard BH emission mechanism and explored observational characteristics of the final burst. Moreover we have also explored and compared PBH burst search methods and differences between a PBH burst and standard cosmological GRBs. Here are the main finding and conclusions of this paper:

1. We have developed improved approximate analytical formulae for the instantaneous BH photon spectrum which includes both the directly Hawking-radiated photons and the photons resulting from the decay or fragmentation and hadronization of other directly Hawking-radiated species. Our analysis incorporates the most recent LHC Standard Model results.
2. For the first time, we have calculated the PBH burst light curve (time profile) and studied its energy dependence both at the source and at the detector.
3. At relatively low energies ($E_\gamma < 10$ TeV), the PBH burst light curve time profile does not show much variation with energy and is well described as a function of remaining burst lifetime by a power law of index ~ -0.7. However, at high energies, the PBH burst light curve profile displays significant variation with energy that may be used as an unique signature of PBH bursts. In addition, at high energies, the light curve profile shows an inflection region around 0.1 s. The HAWC observatory is sensitive in this energy range for a sufficiently nearby PBH and the above features in the light curve may be used to uniquely identify PBH bursts.
4. Compared to the burst Simple Search (photon counting) method, we have found that Maximum Likelihood Search methods using the PBH burst light curve are about 30% more sensitive to PBH bursts. However, we also found that there is not a significant difference in sensitivity between 10-Bin Maximum Likelihood Searches and Unbinned Maximum Likelihood Searches.
5. We have discussed in Section 4.4 the expected differences between PBH bursts and standard cosmological GRBs, in particular that the PBH bursts evolve higher into the TeV band and are typically not expected to be accompanied by an afterglow.
6. We have shown in Section 5 the possibility that evidence of Beyond the Standard Model physics may be discernible in the detector signature of a PBH burst. In particular, a squark state with a rest mass of 5–10 TeV is expected to produce a detectable change in the time dependence of the arrival rate of TeV photons emitted in the final 200 s of the PBH burst.

Acknowledgments

This work was supported by grants from the National Science Foundation (MSU), grant no. PHY-1410972 and Department of Energy (LANL). T.N.U. acknowledges the partial support of this work

by the Laboratory Directed Research and Development (LDRD) program at LANL. We would also like to thank Wade Fisher of MSU for useful conversations on the likelihood fits, Jing-Ya Zhu of MSU for discussions on current models of supersymmetry and Sekhar Chivukula of MSU for useful conversations on Higgs field degrees of freedom and Extra Dimension models. We also thank the anonymous referee for comments that significantly improved the paper.

References

[1] B.J. Carr, K. Kohri, Y. Sendouda, J. Yokoyama, New cosmological constraints on primordial black holes, *Phys. Rev.* D 81 (10) (2010) 104019.
[2] S.W. Hawking, Black hole explosions? *Nature* 248 (1974) 30–31.
[3] J.H. MacGibbon, B.J. Carr, D.N. Page, Do evaporating black holes form photospheres? *Phys. Rev.* D 78 (6) (2008) 064043.
[4] F. Halzen, E. Zas, J.H. MacGibbon, T.C. Weekes, Gamma rays and energetic particles from primordial black holes, *Nature* 353 (1991) 807–815.
[5] K. Griest, M.J. Lehner, A.M. Cieplak, B. Jain, Microlensing of Kepler stars as a method of detecting primordial Black Hole dark matter, Phys. Rev. Lett. 107 (23) (2011) 231101.
[6] A.P. Trofimenko, Black holes in cosmic bodies, *Ap&SS* 168 (1990) 277–292.
[7] D.E. Alexandreas, G.E. Allen, D. Berley, S. Biller, R.L. Burman, M. Cavalli-Sforza, C.Y. Chang, M.L. Chen, P. Chumney, D. Coyne, C. Dion, G.M. Dion, D. Dorfan, R.W. Ellsworth, J.A. Goodman, T.J. Haines, M. Harmon, C.M. Hoffman, L. Kelley, S. Klein, D.E. Nagle, D.M. Schmidt, R. Schnee, C. Sinnis, A. Shoup, M.J. Stark, D.D. Weeks, D.A. Williams, J.P. Wu, T. Yang, G.B. Yodh, W.P. Zhang, New limit on the rate-density of evaporating black holes, Phys. Rev. Lett. 71 (1993) 2524–2527.
[8] M. Amenomori, Z. Cao, B.Z. Dai, L.K. Ding, Y.X. Feng, Z.Y. Feng, K. Hibino, N. Hotta, Q. Huang, A.X. Huo, H.Y. Jia, G.Z. Jiang, S.Q. Jiao, F. Kajino, K. Kasahara, Y. Kitahara, Labaciren, S.M. Liu, D.M. Mei, L. Meng, X.R. Meng, Mimaciren, K. Mizutani, J. Mu, H. Nanjo, M. Nishizawa, A. Oguro, M. Ohnishi, I. Ohta, T. Ouchi, J.R. Ren, T. Saito, M. Sakata, Z.Z. Shi, M. Shibata, T. Shirai, H. Sugimoto, X.X. Sun, K. Taira, Y.H. Tan, N. Tateyama, S. Torii, H. Wang, C.Z. Wen, Y. Yamamoto, G.C. Yu, P. Yuan, C.S. Zhang, H.M. Zhang, L. Zhang, Zhasang, Zhaxiciren, W.D. Zhou, Search for 10 TeV gamma bursts from evaporating primordial Black Holes with the Tibet air shower array, Int. Cosmic Ray Conf. 2 (1995) 112.
[9] E.T. Linton, R.W. Atkins, H.M. Badran, G. Blaylock, P.J. Boyle, J.H. Buckley, K.L. Byrum, D.A. Carter-Lewis, O. Celik, Y.C.K. Chow, P. Cogan, M.K. Daniel, C. Dowdall, A.D. Falcone, D.J. Fegan, S.J. Fegan, J.P. Finley, P. Fortin, K.J. Guiterrez, J. Hall, D. Hanna, J. Holder, D. Horan, S.B. Hughes, T.B. Humensky, I. Jung, G.E. Kenny, M. Kertzman, D.B. Kieda, J. Kildea, J. Knapp, H. Krawczynski, M.J. Lang, S. LeBohec, G. Maier, P. Moriarty, R.A. Ong, J.S. Perkins, F. Pizlo, M. Pohl, J. Quinn, K. Ragan, P.F. Rebillot, P.T. Reynolds, G.H. Sembroski, D. Steele, S.P. Swordy, L. Valcarcel, S.P. Wakely, T.C. Weekes, R.J. White, A new search for primordial black hole evaporations using the Whipple gamma-ray telescope, *JCAP* 1 (2006) 13.
[10] G. Tešić, VERITAS Collaboration, Searching for primordial black holes with the VERITAS gamma-ray experiment, J. Phys. Conf. Ser. 375 (5) (2012) 052024.
[11] J. Glicenstein, A. Barnacka, M. Vivier, T. Herr, for the H. E. S. S. Collaboration, Limits on primordial Black Holeevaporation with the H.E.S.S. array of Cherenkov telescopes, arXiv:1307.4898, (2013).
[12] T.U. Ukwatta, D. Stump, J.T. Linnemann, K. Tollefson, V. Vasileiou, G. Sinnis, J.H. MacGibbon, Milagro limits on the rate-density of primordial Black Holes, Seventh Huntsville Gamma-Ray Burst Symposium, GRB 2013: Paper 44 in eConf Proceedings C1304143, 2013.
[13] A.A. Abdo, A.U. Abeysekara, R. Alfaro, B.T. Allen, C. Alvarez, J.D. Álvarez, R. Arceo, J.C. Arteaga-Velázquez, T. Aune, H.A. Ayala Solares, A.S. Barber, B.M. Baughman, N. Bautista-Elivar, J. Becerra Gonzalez, E. Belmont, S.Y. Ben-Zvi, D. Berley, M. Bonilla Rosales, J. Braun, R.A. Caballero-Lopez, K.S. Caballero-Mora, A. Carramiñana, M. Castillo, G.E. Christopher, U. Cotti, J. Cotzomi, E. de la Fuente, C. De León, T. DeYoung, R. Diaz Hernandez, L. Diaz-Cruz, J.C. Díaz-Vélez, B.L. Dingus, M.A. DuVernois, R.W. Ellsworth, D.W. Fiorino, N. Fraija, A. Galindo, F. Garfias, M.M. González, J.A. Goodman, V. Grabski, M. Gussert, Z. Hampel-Arias, J.P. Harding, E. Hays, C.M. Hoffman, C.M. Hui, P. Hüntemeyer, A. Imran, A. Iriarte, P. Karn, D. Kieda, B.E. Kolterman, G.J. Kunde, A. Lara, R.J. Lauer, W.H. Lee, D. Lennarz, H. León Vargas, E.C. Linares, J.T. Linnemann, M. Longo, R. Luna-Garcla, J.H. MacGibbon, A. Marinelli, S.S. Marinelli, H. Martinez, O. Martinez, J. Martínez-Castro, J.A.J. Matthews, J. McEnery, E. Mendoza Torres, A.I. Mincer, P. Miranda-Romagnoli, E. Moreno, T. Morgan, M. Mostafá, L. Nellen, P. Nemethy, M. Newbold, R. Noriega-Papaqui, T. Oceguera-Becerra, B. Patricelli, R. Pelayo, E.G. Pérez-Pérez, J. Pretz, C. Rivière, D. Rosa-González, E. Ruiz-Velasco, J. Ryan, H. Salazar, F. Salesa, A. Sandoval, P.M. Saz Parkinson, M. Schneider, S. Silich, G. Sinnis, A.J. Smith, D. Stump, K. Sparks Woodle, R.W. Springer, I. Taboada, P.A. Toale, K. Tollefson, I. Torres, T.N. Ukwatta, V. Vasileiou, L. Villaseñor, T. Weisgarber, S. Westerhoff, D.A. Williams, I.G. Wisher, J. Wood, G.B. Yodh, P.W. Younk, D. Zaborov, A. Zepeda, H. Zhou, Milagro limits and HAWC sensitivity for the rate-density of evaporating Primordial Black Holes, Astropart. Phys. 64 (2015) 4–12.
[14] D.N. Page, S.W. Hawking, Gamma rays from primordial black holes, *ApJ* 206 (1976) 1–7.
[15] E.L. Wright, On the density of primordial Black Holes in the Galactic Halo, *ApJ* 459 (1996) 487.
[16] K. Abe, H. Fuke, S. Haino, T. Hams, M. Hasegawa, A. Horikoshi, K.C. Kim, A. Kusumoto, M.H. Lee, Y. Makida, S. Matsuda, Y. Matsukawa, J.W. Mitchell, J. Nishimura, M. Nozaki, R. Orito, J.F. Ormes, K. Sakai, M. Sasaki, E.S. Seo, R. Shinoda, R.E. Streitmatter, J. Suzuki, K. Tanaka, N. Thakur, T. Yamagami, A. Yamamoto, T. Yoshida, K. Yoshimura, Measurement of the cosmic-ray antiproton spectrum at solar minimum with a long-duration balloon flight over Antarctica, Phys. Rev. Lett. 108 (5) (2012) 051102.
[17] J.H. MacGibbon, B.R. Webber, Quark- and gluon-jet emission from primordial black holes: the instantaneous spectra, *Phys. Rev.* D 41 (1990) 3052–3079.
[18] M.W.E. Smith, D.B. Fox, D.F. Cowen, P. Mészáros, G. Tešić, J. Fixelle, I. Bartos, P. Sommers, A. Ashtekar, G. Jogesh Babu, S.D. Barthelmy, S. Coutu, T. DeYoung, A.D. Falcone, S. Gao, B. Hashemi, A. Homeier, S. Márka, B.J. Owen, I. Taboada, The astrophysical multimessenger observatory network (AMON), Astropart. Phys. 45 (2013) 56–70.
[19] A. Keivani, D.B. Fox, G. Tešić, D.F. Cowen, J. Fixelle, AMON searches for jointly-emitting neutrino + gamma-ray transients, arXiv:1508.01315, (2015).
[20] S.W. Hawking, Particle creation by Black Holes, Commun. Math. Phys. 43 (1975) 199–220.
[21] D.N. Page, Particle emission rates from a black hole. II—Massless particles from a rotating hole, *Phys. Rev.* D 14 (1976) 3260–3273.
[22] D.N. Page, Particle emission rates from a black hole. III—Charged leptons from a nonrotating hole, *Phys. Rev.* D 16 (1977) 2402–2411.
[23] D.N. Page, Particle emission rates from a black hole: massless particles from an uncharged, nonrotating hole, *Phys. Rev.* D 13 (1976) 198–206.
[24] T. Elster, Polarisation of the vacuum near a black hole inside a spherical cavity, J. Phys. A Math. Gen. 16 (1983a) 989–996.
[25] T. Elster, Vacuum polarization near a black hole creating particles, Phys. Lett. A 94 (1983b) 205–209.
[26] R.D. Simkins, Massive Scalar Particle Emission from Schwarzschild Black Holes, Pennsylvania State University, University Park, 1986 (Ph.D. thesis).
[27] J. Beringer, J.-F. Arguin, R.M. Barnett, K. Copic, O. Dahl, D.E. Groom, C.-J. Lin, J. Lys, H. Murayama, C.G. Wohl, W.-M. Yao, P.A. Zyla, C. Amsler, M. Antonelli, D.M. Asner, H. Baer, H.R. Band, T. Basaglia, C.W. Bauer, J.J. Beatty, V.I. Belousov, E. Bergren, G. Bernardi, W. Bertl, S. Bethke, H. Bichsel, O. Biebel, E. Blucher, S. Blusk, G. Brooijmans, O. Buchmueller, R.N. Cahn, M. Carena, A. Ceccucci, D. Chakraborty, M.-C. Chen, R.S. Chivukula, G. Cowan, G. D'Ambrosio, T. Damour, D. de Florian, A. de Gouvêa, T. DeGrand, P. de Jong, G. Dissertori, B. Dobrescu, M. Doser, M. Drees, D.A. Edwards, S. Eidelman, J. Erler, V.V. Ezhela, W. Fetscher, B.D. Fields, B. Foster, T.K. Gaisser, L. Garren, H.-J. Gerber, G. Gerbier, T. Gherghetta, S. Golwala, M. Goodman, C. Grab, A.V. Gritsan, J.-F. Grivaz, M. Grünewald, A. Gurtu, T. Gutsche, H.E. Haber, K. Hagiwara, C. Hagmann, C. Hanhart, S. Hashimoto, K.G. Hayes, M. Heffner, B. Heltsley, J.J. Hernández-Rey, K. Hikasa, A. Höcker, J. Holder, A. Holtkamp, J. Huston, J.D. Jackson, K.F. Johnson, T. Junk, D. Karlen, D. Kirkby, S.R. Klein, E. Klempt, R.V. Kowalewski, F. Krauss, M. Kreps, B. Krusche, Y.V. Kuyanov, Y. Kwon, O. Lahav, J. Laiho, P. Langacker, A. Liddle, Z. Ligeti, T.M. Liss, L. Littenberg, K.S. Lugovsky, S.B. Lugovsky, T. Mannel, A.V. Manohar, W.J. Marciano, A.D. Martin, A. Masoni, J. Matthews, D. Milstead, R. Miquel, K. Mönig, F. Moortgat, K. Nakamura, M. Narain, P. Nason, S. Navas, M. Neubert, P. Nevski, Y. Nir, K.A. Olive, L. Pape, J. Parsons, C. Patrignani, J.A. Peacock, S.T. Petcov, A. Piepke, A. Pomarol, G. Punzi, A. Quadt, S. Raby, G. Raffelt, B.N. Ratcliff, P. Richardson, S. Roesler, S. Rolli, A. Romaniouk, L.J. Rosenberg, J.L. Rosner, C.T. Sachrajda, Y. Sakai, G.P. Salam, S. Sarkar, F. Sauli, O. Schneider, K. Scholberg, D. Scott, W.G. Seligman, M.H. Shaevitz, S.R. Sharpe, M. Silari, T. Sjöstrand, P. Skands, J.G. Smith, G.F. Smoot, S. Spanier, H. Spieler, A. Stahl, T. Stanev, S.L. Stone, T. Sumiyoshi, M.J. Syphers, F. Takahashi, M. Tanabashi, J. Terning, M. Titov, N.P. Tkachenko, N.A. Törnqvist, D. Tovey, G. Valencia, K. van Bibber, G. Venanzoni, M.G. Vincter, P. Vogel, A. Vogt, W. Walkowiak, C.W. Walter, D.R. Ward, T. Watari, G. Weiglein, E.J. Weinberg, L.R. Wiencke, L. Wolfenstein, J. Womersley, C.L. Woody, R.L. Workman, A. Yamamoto, G.P. Zeller, O.V. Zenin, J. Zhang, R.-Y. Zhu, G. Harper, V.S. Lugovsky, P. Schaffner, Review of particle physics, *Phys. Rev.* D 86 (1) (2012) 010001.
[28] G. Aad, B. Abbott, J. Abdallah, et. al., Combined measurement of the Higgs Boson mass inpp collisions at s = 7 and 8 TeV with the ATLAS and CMS experiments, Phys. Rev. Lett. 114 (2015) 191803.
[29] M.S. Chanowitz, Electroweak symmetry breaking: unitarity, dynamics, and experimental prospects, Annu. Rev. Nucl. Part. Sci. 38 (1988) 323–420.
[30] M.J. Perry, Black holes are coloured, Phys. Lett. B 71 (1977) 234–236.
[31] D.N. Page, B.J. Carr, J.H. MacGibbon, Bremsstrahlung effects around evaporating black holes, *Phys. Rev.* D 78 (6) (2008) 064044.
[32] D. de Florian, R. Sassot, M. Stratmann, Global analysis of fragmentation functions for protons and charged hadrons, *Phys. Rev.* D 76 (7) (2007) 074033.
[33] S. Albino, B.A. Kniehl, G. Kramer, AKK update: improvements from new theoretical input and experimental data, Nucl. Phys. B 803 (2008) 42–104.
[34] C.T. Hill, Monopolonium, Nucl. Phys. B 224 (1983) 469–490.
[35] C.T. Hill, D.N. Schramm, T.P. Walker, Ultra-high-energy cosmic rays from superconducting cosmic strings, *Phys. Rev.* D 36 (1987) 1007–1016.
[36] T. Sjöstrand, S. Mrenna, P. Skands, A brief introduction to PYTHIA 8.1, Comput. Phys. Commun. 178 (2008) 852–867.
[37] J. Bellm, S. Gieseke, D. Grellscheid, A. Papaefstathiou, S. Platzer, P. Richardson, C. Rohr, T. Schuh, M.H. Seymour, A. Siodmok, A. Wilcock, B. Zimmermann, Herwig++ 2.7 Release Note, arXiv:1310.6877, 2013.
[38] E. Bugaev, P. Klimai, V. Petkov, Photon spectra from final stages of a primordial black hole evaporation in different theoretical models, Int. Cosmic Ray Conf. 3 (2008) 1123–1126.

[39] V.B. Petkov, E.V. Bugaev, P.A. Klimai, M.V. Andreev, V.I. Volchenko, G.V. Volchenko, A.N. Gaponenko, Z.S. Guliev, I.M. Dzaparova, D.V. Smirnov, A.V. Sergeev, A.B. Chernyaev, A.F. Yanin, Searching for very-high-energy gamma-ray bursts from evaporating primordial black holes, Astron. Lett. 34 (2008) 509–514.

[40] HAWC Collaboration, A.U. Abeysekara, R. Alfaro, C. Alvarez, J.D. Álvarez, R. Arceo, J.C. Arteaga-Velázquez, H.A. Ayala Solares, A.S. Barber, B.M. Baughman, N. Bautista-Elivar, E. Belmont, S.Y. BenZvi, D. Berley, M. Bonilla Rosales, J. Braun, R.A. Caballero-Lopez, K.S. Caballero-Mora, A. Carramiñana, M. Castillo, U. Cotti, J. Cotzomi, E. de la Fuente, C. De León, T. DeYoung, R. Diaz Hernandez, J.C. Díaz-Vélez, B.L. Dingus, M.A. DuVernois, R.W. Ellsworth, A. Fernandez, D.W. Fiorino, N. Fraija, A. Galindo, F. Garfias, L.X. González, M.M. González, J.A. Goodman, V. Grabski, M. Gussert, Z. Hampel-Arias, C.M. Hui, P. Hüntemeyer, A. Imran, A. Iriarte, P. Karn, D. Kieda, G.J. Kunde, A. Lara, R.J. Lauer, W.H. Lee, D. Lennarz, H. León Vargas, E.C. Linares, J.T. Linnemann, M. Longo, R. Luna-Garcla, A. Marinelli, H. Martinez, O. Martinez, J. Martínez-Castro, J.A.J. Matthews, P. Miranda-Romagnoli, E. Moreno, M. Mostafá, J. Nava, L. Nellen, M. Newbold, R. Noriega-Papaqui, T. Oceguera-Becerra, B. Patricelli, R. Pelayo, E.G. Pérez-Pérez, J. Pretz, C. Rivière, D. Rosa-González, H. Salazar, F. Salesa, F.E. Sanchez, A. Sandoval, E. Santos, M. Schneider, S. Silich, G. Sinnis, A.J. Smith, K. Sparks, R.W. Springer, I. Taboada, P.A. Toale, K. Tollefson, I. Torres, T.N. Ukwatta, L. Villaseñor, T. Weisgarber, S. Westerhoff, I.G. Wisher, J. Wood, G.B. Yodh, P.W. Younk, D. Zaborov, A. Zepeda, H. Zhou, The HAWC Gamma-Ray Observatory: Dark Matter, Cosmology, and Fundamental Physics„arXiv:1310.0073, 2013.

[41] T.N. Ukwatta, K. Hurley, J.H. MacGibbon, D.S. Svinkin, R.L. Aptekar, S.V. Golenetskii, D.D. Frederiks, V.D. Pal'shin, J. Goldsten, W. Boynton, C. Fellows, K. Harshman, I.G. Mitrofanov, D.V. Golovin, A.S. Kozyrev, M.L. Litvak, A.B. Sanin, A. Rau, A. Kienlin, X. Zhang, M.S. Briggs, V. Connaughton, C. Meegan, K. Yamaoka, Y. Fukazawa, M. Ohno, N. Ohmori, T. Takahashi, M. Tashiro, Y. Terada, T. Murakami, K. Makishima, M. Feroci, F. Frontera, C. Guidorzi, S. Barthelmy, T. Cline, N. Gehrels, J. Cummings, H.A. Krimm, D.M. Smith, J. McTiernan, Investigation of Primordial Black Hole Bursts Using Interplanetary Network Gamma-ray Bursts, arXiv:1512.01264, 2015.

[42] M.G. Hauser, E. Dwek, The cosmic infrared background: measurements and implications, *ARA&A* 39 (2001) 249–307.

[43] MAGIC Collaboration, J. Albert, E. Aliu, H. Anderhub, L.A. Antonelli, P. Antoranz, M. Backes, C. Baixeras, J.A. Barrio, H. Bartko, D. Bastieri, J.K. Becker, W. Bednarek, K. Berger, E. Bernardini, C. Bigongiari, A. Biland, R.K. Bock, G. Bonnoli, P. Bordas, V. Bosch-Ramon, T. Bretz, I. Britvitch, M. Camara, E. Carmona, A. Chilingarian, S. Commichau, J.L. Contreras, J. Cortina, M.T. Costado, S. Covino, V. Curtef, F. Dazzi, A. De Angelis, E.D. Cea del Pozo, R. de los Reyes, B. De Lotto, M. De Maria, F. De Sabata, C.D. Mendez, A. Dominguez, D. Dorner, M. Doro, M. Errando, M. Fagiolini, D. Ferenc, E. Fernández, R. Firpo, M.V. Fonseca, L. Font, N. Galante, R.J. García López, M. Garczarczyk, M. Gaug, F. Goebel, M. Hayashida, A. Herrero, D. Höhne, J. Hose, C.C. Hsu, S. Huber, T. Jogler, T.M. Kneiske, D. Kranich, A. La Barbera, A. Laille, E. Leonardo, E. Lindfors, S. Lombardi, F. Longo, M. López, E. Lorenz, P. Majumdar, G. Maneva, N. Mankuzhiyil, K. Mannheim, L. Maraschi, M. Mariotti, M. Martínez, D. Mazin, M. Meucci, M. Meyer, J.M. Miranda, R. Mirzoyan, S. Mizobuchi, M. Moles, A. Moralejo, D. Nieto, K. Nilsson, J. Ninkovic, N. Otte, I. Oya, M. Panniello, R. Paoletti, J.M. Paredes, M. Pasanen, D. Pascoli, F. Pauss, R.G. Pegna, M.A. Perez-Torres, M. Persic, L. Peruzzo, A. Piccioli, F. Prada, E. Prandini, N. Puchades, A. Raymers, W. Rhode, M. Ribó, J. Rico, M. Rissi, A. Robert, S. Rügamer, A. Saggion, T.Y. Saito, M. Salvati, M. Sanchez-Conde, P. Sartori, K. Satalecka, V. Scalzotto, V. Scapin, R. Schmitt, T. Schweizer, M. Shayduk, K. Shinozaki, S.N. Shore, N. Sidro, A. Sierpowska-Bartosik, A. Sillanpää, D. Sobczynska, F. Spanier, A. Stamerra, L.S. Stark, L. Takalo, F. Tavecchio, P. Temnikov, D. Tescaro, M. Teshima, M. Tluczykont, D.F. Torres, N. Turini, H. Vankov, A. Venturini, V. Vitale, R.M. Wagner, W. Wittek, V. Zabalza, F. Zandanel, R. Zanin, J. Zapatero, Very-high-energy gamma rays from a distant quasar: how transparent is the universe? Science 320 (2008) 1752.

[44] F. Halzen, B. Keszthelyi, E. Zas, Neutrinos from primordial black holes, *Phys. Rev.* D 52 (1995) 3239–3247.

[45] J. Parsons, Extra Dimensions, Particle Data Group Review Article, 2013.

[46] R.S. Chivukula, M. Narain, J. Womersley, Dynamical Electroweak Symmetry Breaking: Implications of the H^0, Particle Data Group Review Article, 2015.

[47] B. Betz, M. Bleicher, U. Harbach, T. Humanic, B. Koch, H. Stöcker, Mini Black Holes at the LHC: Discovery Through Di-Jet Suppression, Mono-Jet Emission and a Supersonic Boom in the Quark-Gluon Plasma in ALICE, ATLAS and CMS, arXiv High Energy Physics—Phenomenology e-prints hep-ph/0606193, 2006.

[48] G. Aad, T. Abajyan, B. Abbott, J. Abdallah, S. Abdel Khalek, O. Abdinov, R. Aben, B. Abi, M. Abolins, O.S. Abouzeid, et al., Search for quantum black hole production in high-invariant-mass lepton+jet final states using pp collisions at $\sqrt{s}$ =8 TeV and the ATLAS detector, Phys. Rev. Lett. 112 (9) (2014) 091804.

[49] ATLAS Collaboration, Search for microscopic black holes and string balls in final states with leptons and jets with the ATLAS detector at sqrt(s) = 8 TeV, arXiv:1405.4254, (2014).

[50] A.F. Heckler, Formation of a Hawking-radiation photosphere around microscopic black holes, *Phys. Rev.* D 55 (1997a) 480–488.

[51] A.F. Heckler, Calculation of the emergent spectrum and observation of primordial black holes, Phys. Rev. Lett. 78 (1997b) 3430–3433.

[52] J. Kapusta, The Last Eight Minutes of a Primordial Black Hole, astro-ph/9911309, 1999.

[53] M.J. Rees, A better way of searching for black-hole explosions, *Nature* 266 (1977) 333.

[54] J.H. MacGibbon, B.J. Carr, Cosmic rays from primordial black holes, *ApJ* 371 (1991) 447–469.

[55] D.B. Cline, B. Czerny, C. Matthey, A. Janiuk, S. Otwinowski, Study of very short gamma-ray bursts: new results from BATSE and Konus, *ApJ Lett.* 633 (2005) L73–L76.

[56] T.N. Ukwatta, P.R. Wozniak, Investigation of Redshift- and Duration-Dependent Clustering of Gamma-ray Bursts, arXiv:1507.07117, 2015.

[57] D.B. Cline, Do very short gamma ray bursts originate from primordial Black Holes? Review, Int. J. Astron. Astrophys. 1 (2011) 164–172.

[58] B. Czerny, A. Janiuk, D.B. Cline, S. Otwinowski, Observational constraints on the nature of very short gamma-ray bursts, New Astron. 16 (2011) 33–45.